# Fast targeting of antigen and surface-derived MHCII into degradative compartments implies endosomal prewiring for antigen presentation in B cells

Running title: **B cell early peripheral MIICs**

Hernández-Pérez S[1*], Vainio M[1*], Kuokkanen E[1], Sustar V[1], Rajala J[1], Paavola V[1], Petrov P[1], Awoniyi LO, Sarapulov AV, Fórsten S[1], Vihinen H[2], Jokitalo E[2], Bruckbauer A[3], and Mattila PK[1]

[1] Institute of Biomedicine, MediCity Research Laboratories, University of Turku, Finland

[2] Institute of Biotechnology, Electron Microscopy Unit, University of Helsinki, Finland

[3] Facility for Imaging by Light Microscopy (FILM), National Heart and Lung Institute, Imperial College London, UK

[*] the authors contributed equally to the study.

**Corresponding author:**

**Pieta Mattila**

Tel: +358 50 574 0780

Fax: +358 2 333 7000

E-mail: pieta.mattila@utu.fi

**Keywords:** Adaptive immune system, B cells, antigen processing, B cell receptor, BCR, MHCII, peptide-loading, endosomes, vesicle traffic

**List of Symbols and Abbreviations used:** BCR, B cell receptor; MHCII, major histocompatibility complex Class II; pMHCII, peptide-MHCII; MIIC, MHCII peptide-loading compartment; SDCM, spinning disk confocal microscopy; EE, early endosome; LE, late endosome; RE, recycling endosome; CatS, cathepsin S

## Abstract

In order to mount high-affinity antibody responses, B cells internalise specific antigens and process them into peptides loaded onto MHCII for presentation to $T_H$ cells. While the biochemical principles of antigen processing and MHCII loading have been well dissected, how the endosomal vesicle system is wired to enable these specific functions remains much less studied. Here, we performed a

systematic microscopy-based analysis of antigen trafficking in B cells to reveal its route to the MHCII peptide-loading compartment (MIIC). Surprisingly, we detected fast targeting of internalised antigen into peripheral acidic compartments that possessed the hallmarks of MIIC and also showed degradative capacity. In these vesicles, internalised antigen converged rapidly with membrane-derived MHCII and partially overlapped with Cathepsin-S and H2-M, both required for peptide loading. These early compartments appeared heterogenous and atypical as they contained a mixture of both early and late markers, indicating specialized endosomal route. Together, our data suggests that, in addition to previously-reported perinuclear late endosomal MIICs, antigen processing and peptide loading could start already in these specialized early peripheral acidic vesicles to support fast peptide-MHCII presentation.

## Introduction

B lymphocytes (B cells) are an essential part of the adaptive immune system, initiating antibody responses against a vast repertoire of different antigens. Critical for the ability of B cells to mount a mature antibody response including class-switch recombination and affinity maturation, is the presentation of specific antigen-derived peptides loaded onto the major histocompatibility complex (MHC) class II (MHCII). Presentation of peptide-MHCII (pMHCII) complex on the B cell surface enables them to act as antigen-presenting cells (APCs) to CD4+ T lymphocytes (T helper cells, $T_H$ cells). T cell receptor (TCR)-pMHCII interaction provides a second activation signal to the B cells. Reciprocally, pMHCII presented on B cells stimulates cognate $T_H$ cells to orchestrate other branches of the immune system and to generate CD4+ T cell memory (Whitmire et al., 2009).

Presentation of different antigenic peptides on MHCII is a critical driver of various adaptive immune responses. Other professional APCs, such as dendritic cells and macrophages, present peptides from unspecified antigens taken up by phagocytosis or via receptor-mediated uptake of innate type of immune receptors, like complement receptors or Fc-receptors. B cells, however, ensure efficient presentation of antigens of given specificity, determined by the B cell antigen receptor (BCR) (Aluvihare et al., 1997; Unanue et al., 2016). Studies on pMHCII loading have largely focused on dendritic cells and macrophages, leaving B cell antigen processing and presentation less understood.

The MHCII peptide-loading compartment (MIIC), where antigen is processed into peptides for loading onto MHCII molecules, contains in addition to its main hallmarks, antigen and MHCII, the key peptide loading chaperone H2-M and the proteolytic enzyme Cathepsin-S (Adler et al., 2017). MIIC has been well characterized by various biochemical fractionation techniques. However, in these assays the information about the heterogeneity, localization and dynamics of the vesicles is typically lost. Therefore, important questions remain about the coordination of antigen processing and MHCII loading and presentation. How is the endosomal vesicle machinery of B cells tuned to enable this highly specific process and how is the efficient targeting of BCR-derived antigen for processing coordinated? It has been suggested that MIICs are multivesicular and typically contain a late endosomal / lysosomal marker Late Antigen Membrane Protein 1 (LAMP1) (Lankar et al., 2002; Unanue et al., 2016; Adler et al., 2017). Thus, a picture has been outlined where the maturation of MIIC diverts at the stage of multivesicular bodies (MVB) before fusion with end-stage lysosome. However, it is not understood how this process is regulated. To help to decipher the molecular underpinnings of antigen presentation, deeper knowledge on intracellular trafficking of antigen would be required.

78 In the last 10-15 years, developments in fluorescence microscopy techniques, including improved
79 fluorophores and fluorescent fusion proteins, as well as more sensitive and higher resolution imaging
80 modalities, have significantly increased our general understanding of intracellular vesicle traffic.
81 Microscopy can provide information about the dynamics and heterogeneity of different vesicle
82 carriers that are otherwise challenging to decipher with other techniques. The classical or ubiquitous
83 endolysosomal pathway is delineated as a route from early endosomes (EE) to late endosomes (LE)
84 / MVB and, lastly, to lysosomes, with early and late recycling endosomes (RE) sending cargo back
85 to the cell surface. While this general view is relatively well established, new studies continue to
86 reveal dramatic complexity within the endolysosomal system with numerous vesicle sub-populations,
87 transport proteins and vesicle markers as well as vesicle scission and fusion machineries (Chen et al.,
88 2019; Delevoye et al., 2019; Huotari and Helenius, 2011). A group of vital regulators of vesicle traffic
89 are the small GTPases of the Rab protein family that are widely used to define different
90 endolysosomal sub-populations. This family contains more than 60 proteins in humans performing
91 either ubiquitous or specific functions in vesicle traffic (Wardinger-Ness & Zerial, 2014). The
92 appreciation of the role of the Rab proteins has been key in unravelling the endosomal network
93 dynamics. However, different carriers vary not only in terms of their Rab identity markers, but also
94 in size, shape, membrane morphology, subcellular localization and acidity. In addition, identification
95 of different cell-type specific variations of vesicular transport systems and diverse specialized
96 endolysosome-related organelles, where MIIC could be counted in (Delevoye et al., 2019), pose an
97 ongoing challenge for researchers.
98
99 In this work, we set up a systematic microscopy approach to follow how antigen, after BCR-mediated
100 internalisation, traffics into MIIC. In accordance to previous studies, we detected and quantified
101 gradual clustering of antigen vesicles towards perinuclear region in 30-60 min. Right after
102 internalisation, antigen appeared in heterogenous vesicles that harboured mixed selection of both
103 early and late endosomal markers. Interestingly, already these early compartments in the cell
104 periphery accumulated hallmarks of MIIC and were able to gain degradative capacity. By specific
105 visualization of membrane-derived MHCII molecules, we found that in these early antigen
106 compartments, MHCII originated largely from the plasma membrane pool, possibly to support fast,
107 first-wave peptide presentation. This study provides the first in-depth imaging of antigen processing
108 pathway in B cells. We found remarkable efficiency in joint targeting of antigen and membrane-
109 derived MHCII into peripheral compartments with hallmarks of MIIC. The results increase our
110 understanding of the endolysosomal machinery responsible for MIIC formation and can facilitate
111 future dissections of the regulation of successful antigen presentation.

112 **Results**

113

114 ***Antigen migrates into the perinuclear area in 30-60 min after activation***

115 To characterize antigen vesicle trafficking in B cells, we first set to analyse the migration and
116 clustering of antigen in a quantitative manner. We used cultured A20 B cells expressing transgenic
117 D1.3 IgM (A20 D1.3) and activated them with Alexa Fluor-labelled anti-IgM antibodies (AF-αIgM)
118 as surrogate antigen. The localization of the antigen vesicles was imaged in cells fixed at different
119 timepoints and stained for pericentriolar material 1 (PCM1) as a marker for microtubule organizing
120 centre (MTOC) by spinning disc confocal microscopy (SDCM). Well consistent with the literature
121 (Aluvihare et al., 1997; Siemasko et al., 1998; Tsui et al., 2018; Vascotto et al., 2007a), we found
122 that, within 30-60 min, most cells gathered antigen in a cluster that typically localized quite centrally
123 in the vicinity of MTOC (Fig. 1A). The same phenomenon was also detected in splenic primary B
124 cells isolated from MD4 mouse strain, selected for their relatively high and homogenous levels of
125 IgM. Primary B cells, however, showed faster kinetics with most cells accumulating antigen in central
126 clusters already in less than 30 min (Fig. 1B). To quantitatively analyse antigen migration, we
127 deconvolved the images to improve the separation of small vesicles and then quantified the total
128 number of vesicles per cell and their mean distance to the MTOC using MatLab-based 3D analysis
129 (Fig. 1C). By showing a reduction of the vesicle numbers over time, the analysis clearly demonstrated
130 the fusion, or clustering, of vesicles into bigger entities. At the same time, the average distance to the
131 MTOC decreased, depicting migration of the vesicles closer to the MTOC over time (Fig. 1D, E).
132 Although the vesicle number diminished between 30 and 45 min, the mean distance of the vesicles
133 to the MTOC remained constant. This suggested that the majority of the antigen was trafficked to the
134 perinuclear region already in 30 min, but vesicle fusion events and/or clustering continued at later
135 timepoints (Fig. 1E). The quantification revealed the overall kinetics of the antigen transition from
136 smaller peripheral vesicles into bigger vesicles or vesicle clusters that accumulate close to the MTOC.

137

138 In order to gain insights into the morphological features of the antigen vesicles, we activated the A20
139 D1.3 cells with a mixture of AF-αIgM and 6 nm-colloidal gold-αIgM and used transmission electron
140 microscopy (TEM) to visualize antigen-containing membrane structures. We found high
141 heterogeneity in the vesicle morphologies both after 15 min of activation and after 75 min of
142 activation when the antigen was largely concentrated in the middle of the cells (Fig. 1F). In the 15
143 min timepoint, we found antigen in spherical or horse-shoe shaped single membrane vesicles, as well
144 as in tubular or network-like structures, which often contained intralumenal vesicles (Fig. 1F;

145 Supplementary Fig. 1A). MVBs are typically considered to represent late endosomes, and for MIICs,
146 MVB-like structures have been characterized after 1h of activation in the perinuclear region (Adler
147 et al., 2017; Lankar et al., 2002; Unanue et al., 2016; Vascotto et al., 2007b). While multivesicular
148 morphology has been linked to MHCII loading (Roche and Furuta, 2015; Lith et al., 2001; Xiu et al.,
149 2011), the localization of antigen into multivesicular structures raised the question whether already
150 at 15 min after activation, in the cell periphery, antigen could be in MIIC. At 75 min timepoint, we
151 found antigen predominantly in multivesicular structures accumulated in the perinuclear area. This
152 region was also very dense in various other membrane organelles, such as Golgi and mitochondria.
153 Consistent with the literature (Vascotto et al., 2007a), we also typically found these vesicle-dense
154 areas at sites of nuclear invaginations (Fig. 1F). The possible effect of colloidal gold-conjugation to
155 the localization of anti-IgM was controlled by immunofluorescence analysis of sample duplicates.
156 We detected strong colocalisation of fluorescently labelled anti-IgM and gold-conjugated anti-IgM,
157 distinguished by a specific secondary staining. Both antigens also accumulated together into
158 perinuclear Rab7 compartment at 75 min timepoint similarly to the samples without colloidal gold
159 (Supplementary Fig. S1B; see Fig. 1A and Fig. 2B).
160
161 ***Antigen colocalisation with early and late endosomal Rab-proteins***
162 Mechanisms of endosomal trafficking in various cellular systems are largely governed by Rab-family
163 of small GTPases, which are commonly used to define sub-populations of vesicles with different
164 functions. To reveal the endolysosomal character of the vesicles transporting antigen, we designed a
165 series of colocalisation analyses with the following classical endosomal markers: Rab5 for EEs, Rab7
166 and Rab9 for LEs and lysosomes, and Rab11 for REs. As antigen-bound BCR is known to form
167 clusters at the cell membrane prior to endocytosis, we first examined the proportion of the dot-like
168 antigen features that was internalised at 10-20 min timepoints, and thus would be expected to
169 colocalise with vesicular markers. At these early timepoints most vesicles still remain in the cell
170 periphery and it is not readily apparent if the antigen is internalised or just clustered at the plasma
171 membrane. To distinguish the internalised antigen from the antigen still on the plasma membrane, we
172 stimulated the cells with biotinylated AF-αIgM. After 10-60 min activation, cells were stained on ice
173 with fluorescent streptavidin and fixed (Supplementary Fig. S2A). In this way, we were able to
174 distinguish between total (Alexa Fluor 647) and membrane-exposed (Alexa Fluor 488) antigen. We
175 saw that in 10-20 min, approximately 40-50% of the dotted antigen features in the images represented
176 internalised vesicles, while the rest of the signal originates from antigen that still remains at the cell
177 surface. As expected, at later timepoints (60 min), majority of the antigen pool was detected inside
178 the cells (Supplementary Fig. S2B, C). This was well consistent with the flow cytometric analysis of

179 antigen internalisation (Supplementary Fig. S2D). Consistently, we also frequently found non-
180 internalised antigen at the plasma membrane in TEM samples after 15 min of activation
181 (Supplementary Fig. S1A).
182
183 To study the colocalisation of antigen and different vesicle markers, we performed
184 immunofluorescence analysis with SDCM. We expected to see clearly higher colocalisation of
185 antigen with early endosomal Rab5 in the early timepoints, and with late endosomal markers at later
186 timepoints. To our surprise, we did not detect major differences between the markers. Instead, Rab5,
187 Rab7, Rab9 and Rab11 all showed prominent punctate pattern of vesicles very close to the plasma
188 membrane that partially overlapped with antigen and partially located just underneath the antigen
189 signal (Fig. 2A, C; Supplementary Fig. S3A). As a negative control, we used Golgi-specific transport
190 protein Rab6 and, as expected, it showed no notable colocalisation with antigen. We quantified the
191 colocalisation using Manders´ overlap coefficient, split for antigen channel (M2) (Manders et al.,
192 1993), using Huygens software with automated thresholding. M2 measures the portion of antigen that
193 overlaps with the signal from different Rab-proteins. The analysis supported partial colocalisation of
194 antigen with Rab5, Rab7, Rab9 and Rab11, already at early timepoints after activation (Fig. 2C).
195
196 At 60 min timepoint, when most of the antigen was clustered in the perinuclear region, we found
197 enhanced colocalisation with late endosomal markers Rab7 and Rab9, as expected (Fig. 2B,
198 Supplementary Fig. S3B). Rab11, involved in slow recycling, also localized to the antigen cluster as
199 well as the early endosomal marker Rab5. The negative control, Rab6, was found in the perinuclear
200 region close to antigen but with very limited overlap in signals. This suggested translocation of the
201 antigen close to the Golgi apparatus, supporting the above observed localization close to the MTOC
202 (Fig. 1). The quantification suggested significant overlap of antigen with all the studied Rab-proteins
203 except Rab6, with an increasing trend over time (Fig. 2C).
204
205 Majority of the vesicles were found very close to each other, both at the early and late time points, at
206 the vicinity of the plasma membrane or in the perinuclear region, respectively, leading to
207 overestimation of the signal overlap. In order to improve the resolution of our data and to better
208 separate different vesicles, we employed super-resolution radial fluctuations (SRRF), an imaging
209 method based on post-processing analysis of signal fluctuations (Gustafsson et al., 2016). Here, we
210 analysed samples activated for 10 or 45 min in order to resolve the nature of the antigen vesicles in
211 the perinuclear region. Super-resolution SRRF images were obtained by taking 20-50 repetitive
212 images of the same field of view with SDCM and post-processing the data using SRRF plugin in

213 ImageJ. In this way, we could improve the separation of the vesicles significantly and now detected
214 more distinct differences in the localization of Rab-proteins with respect to antigen, especially in later
215 timepoints. In 45 min, Rab7 and Rab9 showed clear colocalisation with antigen, as expected for their
216 late endosomal nature, while Rab5 and Rab11 appeared more scattered and only partially colocalised
217 with antigen, often marking vesicles or membrane domains adjacent to it (Fig. 2D). We analysed
218 SRRF images for Manders´ overlap coefficient (M2) and detected a marked colocalisation of antigen
219 signal with late endosomal markers Rab7 and Rab9 in 45 min. We also detected overlap with Rab11,
220 and, to some extent, with Rab5. However, in 10 min the analysis showed close to equal colocalisation
221 of Rab5, Rab7 and Rab9, and a modest level of colocalisation with Rab11. Colocalisation of antigen
222 with Rab6 remained low, confirming the specificity of the analysis (Fig. 2E). The presence of Rab11
223 in the antigen vesicles could suggest fission and recycling, to some extent already at early timepoints
224 but with increasing efficiency towards later timepoints.
225
226 ***Antigen trafficking involves atypical vesicles that share both early and late endosomal character***
227 To better define antigen transport vesicles, we asked how other typical early and late endosomal
228 markers, Early Endosome Antigen 1 (EEA1) and LAMP1, respectively, correlated with antigen at
229 different timepoints. Consistent with the data on different Rab-proteins, we detected partial
230 colocalisation of antigen with both EEA1 and LAMP1 already at early timepoints (Fig. 3A,
231 Supplementary Fig. S3C). The colocalisation became more prominent as antigen trafficked to the
232 perinuclear region (Fig. 3B, Supplementary Fig. S3D). Manders´ overlap coefficient also showed
233 continuous or perhaps even increasing overlap with antigen for both markers (Fig. 3C). However,
234 Pearson´s correlation coefficients for EEA1 and LAMP1 crossed over time indicating that
235 significantly higher proportion of LAMP1 compared to EEA1 colocalised with antigen at later
236 timepoints. This is consistent with a high proportion of EEA1 endosomes remaining in the cell
237 periphery, while some coalesce in the central cluster together with antigen, as shown by the M2. On
238 the other hand, increasing proportion of LAMP1-positive vesicles accumulated in the perinuclear
239 region with antigen over time.
240
241 As a complementary approach, we again turned to SRRF super-resolution analysis in order to achieve
242 higher accuracy. We examined the colocalisation of antigen with EEA1 and LAMP1 at 10 and 45
243 min after activation. SRRF analysis confirmed higher colocalisation of antigen with EEA1 compared
244 to LAMP1 in the early timepoints (10 min), and vice versa after 45 min (Fig. 3D-E). Nevertheless,
245 EEA1 colocalisation with antigen was also detected both in some remaining peripheral vesicles and
246 in the perinuclear antigen vesicle cluster, raising a possibility that also early endosomal EEA1 could

247 indeed localize to the MIIC. Together, this data revealed surprising localization of antigen with not
248 only early, but also late endosomal carriers shortly after internalisation. At later timepoints, close to
249 the MTOC, preference for late endosomal / lysosomal markers was notable, yet also early endosomal
250 markers were found to overlap with antigen.
251
252 As previous shown (Supplementary Fig. S2B-C), in 15 min approximately half of the dots with
253 antigen signal should represent vesicles inside the cell, and the rest should originate from antigen-
254 BCR clusters still at the plasma membrane. Therefore, M2 values for one type of vesicle marker
255 should not be considerably higher than 50% in the early timepoints. Our observation that antigen
256 showed an overlap of 40-60% with both early and late endosomal markers can simply reflect technical
257 challenges to resolve small vesicles close to each other, causing adjacent vesicles to appear as
258 colocalised. Additionally, it could point towards mixed vesicle identities that would simultaneously
259 possess both early and late markers. To test for these two non-exclusive scenarios, we next performed
260 SRRF super-resolution analysis on cells activated either for 10 or 45 min and stained for LAMP1 and
261 EEA1, and asked if the markers colocalised in the same antigen vesicles. We found antigen vesicles
262 that colocalised with only either EEA1 or LAMP1, but we also found several prominent vesicles that
263 clearly contained both markers simultaneously (Fig. 3F).
264
265 Next, we asked if the vesicles that share both early and late endosomal markers were in the transition
266 state of their maturation or if they represented a special compartment. To investigate this, we
267 performed live imaging of A20 D1.3 B cells transfected with green fluorescent protein (GFP)-fused
268 Rab5 and loaded with LysoTracker, a fluorescent tracer that labels low pH compartments, such as
269 LEs and lysosomes. We followed antigen vesicles at early timepoints after internalisation by SDCM.
270 We detected several antigen vesicles that contained both early endosomal Rab5 and LysoTracker
271 (Fig. 3G; Supplementary Movie 1). The joint movement of the markers implied physical
272 colocalisation, and indicated that antigen, indeed, traffics in atypical vesicles that share both early
273 and late endosomal features. Interestingly, we detected double positive vesicles also before cell
274 activation (Supplementary Fig. 4).
275
276 ***Antigen enters degradative compartments shortly after internalisation***
277 As the primary purpose of antigen uptake by B cells is to degrade it for loading the resulting peptides
278 onto MHCII complexes, we next asked the question where and when does the antigen degradation
279 start. We linked a fluorescent probe for proteolysis, DQ-OVA, to αIgM or specific HEL antigen
280 recognized by the D1.3 BCR (Fig. 4A). Fluorescent DQ moieties quench each other when the probe

281 remains intact. However, upon proteolysis the quenching ceases and the fluorescence can be detected.
282 We first analysed the increase in DQ fluorescence by flow cytometry. Already at 15-20 min we
283 detected a clear signal that constantly increased through the analysis period, 45 min, suggesting that
284 the proteolysis starts relatively fast after antigen uptake (Fig. 4B). We detected brighter DQ-Ova
285 signal at later timepoints when linked to HEL, despite having similar internalisation rate to anti-IgM
286 (see Supplementary Fig. S2D). Due to the brighter signal of DQ-Ova conjugated to HEL, we
287 performed the microscopy analysis using this probe. Fluorescence signal from antigen-linked DQ
288 moieties was also visible by microscopy at 20 min after activation. The DQ-signal overlapped well
289 with EEA1 and was also found to colocalise with CatS, an enzyme essential for preparing the MHCII
290 for peptide loading (Fig. 4C).
291
292 To investigate the level of antigen colocalisation with CatS in a more comprehensive way, we
293 performed immunofluorescence analysis in cells activated for 10 or 45 min. Conventional SDCM
294 imaging suggested partial colocalisation of CatS with antigen both at 10 and 45 min timepoints (Fig.
295 4D, upper panel). In order to resolve the vesicles better, we performed SRRF analysis, and could
296 more unambiguously detect antigen vesicles that clearly contained CatS already 10 min after
297 activation (Fig. 4D, middle panel). Interestingly, the colocalisation level remained roughly similar,
298 although low, in the later timepoints in the perinuclear region (Fig. 4D, bottom panel; Supplementary
299 Fig. 5A).
300
301 Proteolytic activity typically requires acidic pH of the vesicles. To examine the pH of the antigen
302 vesicles, we used live imaging with LysoTracker, as its accumulation is based on acidic pH. In line
303 with our data above (Fig. 3G), we found strong colocalisation of antigen with LysoTracker already
304 in the very early timepoints (1-5 min after activation) (Fig. 4E; Supplementary Movie 2). Notably,
305 we also detected antigen fusing with LysoTracker positive vesicles immediately after internalisation,
306 indicating very fast and efficient targeting of antigen to acidic vesicles (Fig. 4F; Supplementary
307 Movie 3). Curiously, LysoTracker positive vesicles appeared to hover beneath the plasma membrane
308 ready to catch the internalised antigen.
309
310 ***Antigen colocalises with plasma membrane derived MHCII rapidly after internalisation***
311 The data above suggests that antigen processing could be initiated already in the peripheral antigen
312 vesicles shortly after internalisation. To ask if these early peripheral vesicles might represent MIIC,
313 we asked whether they also contain MHCII. We activated the cells for 10 or 60 min with fluorescent
314 antigen and performed immunofluorescence staining of total MHCII. As expected, we found MHCII

315 to strongly colocalise with antigen in the perinuclear antigen cluster at 30 min timepoint.
316 Interestingly, after 10 min of activation, we also detected MHCII in various intracellular vesicles
317 including those containing antigen (Supplementary Fig. S5B). Due to the high signal originating from
318 the plasma membrane-resident MHCII and several internal MHCII-positive structures, we decided to
319 analyse the samples with a super-resolution technique structured illumination microscopy (SIM).
320 SIM significantly improved the resolution and clarity of the imaging (x-y-z), and we could detect
321 strong colocalisation of antigen and MHCII in clearly defined vesicles already at 15 min after cell
322 activation (Fig. 5A).
323
324 To investigate if the MHCII in the early antigen vesicles was newly synthesized from the trans-Golgi
325 network, or originated from the plasma membrane pool, we prelabelled the surface MHCII prior to
326 cell activation (Fig. 5B). Interestingly, we saw a strong localization of surface-derived MHCII
327 (sMHCII) to early peripheral antigen vesicles (Fig. 5C). We then proceeded to verify the
328 colocalisation by performing live imaging of cells labelled with fluorescent anti-MHCII prior to
329 activation with fluorescent antigen. The movies revealed very high level of sMHCII in the antigen
330 vesicles (Fig. 5D, Supplementary Movie 4). Finally, to further prove that the early peripheral antigen
331 vesicles could function as MIIC, we stained the cells for H2-M, a molecule of MHC family that
332 functions as a key chaperone in peptide loading to MHCII (Mellins and Stern, 2014). Notably, SRRF
333 super-resolution imaging of immunofluorescence samples showed clear colocalisation of antigen
334 vesicles and H2-M already at 15 min after activation further supporting classification of these early
335 peripheral antigen vesicles as MIIC (Fig. 5E; Supplementary Fig. 5C).
336
337 **Discussion**
338
339 BCR-mediated uptake of specific antigens and their processing for pMHCII presentation is crucial
340 for T cell-dependent antibody responses and BCR/antibody affinity maturation in the germinal
341 centres. Different microscopy-based methods have become a critical tool in studying complicated
342 vesicular networks and can now be used to tackle the endolysosomal system governing antigen
343 processing in B cells. Here, we combined systematic colocalisation analysis of antigen with key
344 markers of various endolysosomal compartments and known components of MIIC to gain
345 information on antigen trafficking towards processing compartments. Consistent with previous
346 studies (Aluvihare et al., 1997; Siemasko et al., 1998; Vascotto et al., 2007a), we observed that, over
347 time, antigen concentrates in the perinuclear region together with late endosomal markers LAMP1,
348 Rab7 and Rab9, in compartments well-fitting to the description of MIIC. However, we also saw fast

349 and highly efficient targeting of antigen into acidic compartments, that also possessed key features
350 of MIIC, already in minutes after internalisation. These vesicles located in the cell periphery,
351 displayed a heterogenous combination of early and late endosomal markers and also exhibited
352 variable ultrastructural morphologies. Interestingly, we show robust recruitment of surface-derived
353 MHCII to these early peripheral MIICs suggesting that they could support fast presentation using
354 MHCII recycled from the plasma membrane. This work provides the first endosomal roadmap of the
355 intracellular trafficking of antigen in B cells and reveals previously unappreciated efficacy in MIIC
356 formation.
357
358 Much of our knowledge in B cell antigen processing compartments is derived from biochemical
359 studies, including cell fractionations, radiolabelling of antigen, and electron microscopy (Amigorena
360 et al., 1994; Lankar et al., 2002; West et al., 1994). While already these early studies drew a valid
361 picture of late endosomal or lysosomal, i.e. LAMP1-positive, multivesicular compartment, the
362 approaches were not suitable to address questions about intracellular localization or dynamics of the
363 antigen vesicles. Yet, these features have been strongly linked to distinct functional properties of
364 endolysosomes and they also inform us about the possible molecular machineries regulating the
365 vesicle traffic (Huotari and Helenius 2011; Hutagalung and Novick, 2011). Our microscopic analysis
366 revealed a remarkable heterogeneity in the endolysosomal markers of antigen vesicles (Fig. 1-3).
367 However, overlapping fluorescent signals could be derived from a vesicle containing two markers,
368 two vesicles containing different markers, or a multilobular vesicle with distinct markers in different
369 domains, not resolvable by conventional light microscopy. Therefore, the small size and crowdedness
370 of the vesicles generated challenges for the colocalisation analyses, which we could, at least partially,
371 overcome by the super-resolution SRRF and SIM analyses. While SDCM can achieve a lateral
372 resolution of 250-300 nm, SIM and SRRF improve the x-y resolution by approximately 2-fold. SIM
373 also improves the axial resolution by 2-fold from approximately 600 to 300nm.
374
375 The vesicle heterogeneity could be linked to the notion that antigen enters vesicles with low pH
376 (LysoTracker-positive) and degradative capacity (demonstrated by DQ-Ova signal and partial
377 overlap with CatS) extremely fast after internalisation (Fig. 4). It has also been shown that the
378 amounts of Rab-proteins on a given vesicle can fluctuate, increasing the noise in the colocalisation
379 parameters (Huotari and Helenius 2011; Hutagalung and Novick, 2011; Rink et al. 2005; Vonderheit
380 and Helenius 2005). Notably, we found that antigen also trafficked in atypical vesicles stably marked
381 by both early endosomal Rab5 and LysoTracker indicating that the heterogeneity of the vesicles
382 would be a more constant feature and not a mere transition state. Our data does not clearly fit the

383 classical “Rab conversion” model, where a vesicle rapidly shifts from Rab5-positive into Rab7-
384 positive (Huotari and Helenius, 2011; Hutagalung and Novick, 2011). Instead, the data might better
385 comply with an alternative model, where sequential budding of membrane domains with late
386 endosomal markers would occur from early/sorting endosomes (Huotari and Helenius 2011;
387 Wandinger-Ness and Zerial, 2014) and, indeed, we often detected adjacent localization of different
388 markers possibly indicative of distinct domain on the same vesicle.
389
390 Martinez-Martin and colleagues used SIM to demonstrate, in primary B cells, that 15 min after
391 activation, part of the internalised antigen concentrated in ring-like structures representing
392 autophagosomes (Martinez-Martin et al., 2017). However, it remains unclear what could be the role
393 of autophagy in terms of antigen fate or pMHCII processing. In our SIM analysis, we also detected
394 some ring-like structures, that could represent autophagosomes (Fig. 5A) and the partial partitioning
395 of antigen in these autophagosomes could be responsible for some of the vesicle heterogeneity we
396 observed. Our data also does not rule out contribution of other vesicular carriers, like clathrin-
397 independent carriers (CLICs), that do not contain specific markers (Kirkham et al., 2005).
398
399 An interesting finding from our live imaging data was that the LysoTracker positive, i.e. low pH
400 vesicles, appeared to hover close to the plasma membrane and capture antigen right after
401 internalisation (Fig. 4F). Some of these LysoTracker-positive vesicles also contained Rab5 already
402 before cell activation (Supplementary Fig. S4). This effectiveness suggests prewiring of the B cells
403 endolysosomal system towards antigen presentation, probably accompanied or boosted by a
404 signalling component from the BCR, as suggested already by Siemasko and colleagues (Siemasko et
405 al., 1998). As such, we support MIIC to be considered as a member of the growing family of
406 specialized endolysosome-related organelles (ELRO) with diverse functions, as proposed in a recent
407 review by Delevoye and colleagues (Delevoye et al., 2019). Considering the poor compliance of
408 antigen vesicles with classical endolysosomal pathway, other ELROs could serve as valuable
409 additional points of comparisons for studies of MIIC membrane traffic. It has been shown that B cells
410 on activatory surfaces mimicking immunological synapses, polarize the MTOC and acidic MHCII
411 vesicles to secrete proteases for antigen extraction (Yuseff et al., 2011). While this happens at later
412 stages of activation and is proposed to precede antigen internalisation, it demonstrates atypical
413 functions of B cell acidic compartments, perhaps analogous to the secretion of lytic granules, another
414 type of ELRO, by CD8+ T cells (Delevoye et al., 2019; Yuseff et al., 2013).
415

416 To test if antigen trafficking, despite of the observed heterogeneity, would depend on the classical
417 early and late endosomal Rabs, we expressed various dominant negative or constitutively active
418 mutants of Rab 5, 7, 9 and 11, but were not able to detect clear defects in antigen migration patterns
419 (data not shown). This could point towards a hitherto unknown hardwiring in the system making these
420 regulators redundant. Alternatively, the Rab mutants might not function as expected, as soundly
421 demonstrated for the commonly used activating mutations that might not get activated in the first
422 place (Langemeyer et al., 2014). In addition, redundancy is likely between isoforms and paralogs,
423 like Rab5 isoforms a/b/c, or Rab7 and Rab9 which share high sequence homology and are suggested
424 to play mutually redundant roles (Homma et al., 2019). Numerous other Rab-proteins have been
425 shown to possess cell type or cargo-specific functions, linked to different ELROs. It is well possible
426 that other Rab-proteins, not tested in this study, could serve as critical regulators of antigen vesicle
427 trafficking. In dendritic cells, a genome-wide siRNA screen for molecules regulating MHCII
428 distribution, has been performed (Paul et al., 2011). This screen did not highlight any Rab-family
429 proteins, suggesting for considerable redundancy in the pathway.
430
431 Early biochemical studies, using lipopolysaccharide-activated B lymphoblasts, have proposed the
432 existence of peptide-loaded MHCII in multiple endolysosomal compartments (Castellino and
433 Germain, 1995) and, using the same B cell line than us, demonstrated that B cells can indeed present
434 antigen already in 20 min after activation (Aluvihare et al., 1997). Furthermore, studies have shown
435 antigen degradation into peptides 20 min after activation (Barroso et al., 2015; Davidson et al., 1990).
436 These studies are consistent with our finding that the internalised antigen vesicles highly efficiently
437 colocalise with MHCII in various compartments, as well as partially overlap with Cathepsin-S and
438 H2-M (Fig. 4-5). The degradative capacity of the early peripheral vesicles (Fig. 4-5) further supports
439 function in antigen processing. Interestingly, we found that the newly internalised antigen robustly
440 co-localized with surface-derived MHCII (Fig. 5), suggesting that the pre-existing pool of MHCII
441 could be used for the first wave of pMHCII presentation. This point has been previously tested using
442 cycloheximide, known to block de novo protein synthesis. There, however, cycloheximide was found
443 to inhibit all presentation and it was interpreted so that B cells could only present peptides on newly
444 synthesized MHCII (Aluvihare et al., 1997). Later, concerns have been raised on the side effects of
445 cycloheximide. These include disturbance of endosomal trafficking, actin cytoskeletal dynamics and
446 cell polarization and motility (Clotworthy and Traynor, 2006; Darvishi and Woldemichael, 2016;
447 Oksvold et al., 2012). Thus, the old findings with cycloheximide warrant for a revisit with a sensitive
448 pulse assay for antigen presentation together with more specific inhibitors like, for example, the
449 newly developed FLI-06 that targets ER-exit sites and trans-Golgi network (Yonemura et al., 2016).

450 Our suggestion that biosynthetic MHCII probably arrives to MIIC at later stages, is supported by the
451 old metabolic labelling studies, where, again using the same B cell line than in our study, it was
452 shown that the newly synthesized MHCII arrives to MIIC in 30-60 min after cell activation
453 (Amigorena et al., 1994).
454
455 The early peripheral MIICs could facilitate the speed of pMHCII presentation but could also tune the
456 peptide repertoire. In cell fractionation studies, an MHC class II-like protein H2-O has been reported
457 to concentrate more with the early endosomal fraction as compared to late endosomal fraction, while
458 the peptide-loading chaperone H2-M shows the opposite trend (Gondré-Lewis et al., 2001). While
459 H2-O has been characterized with an inhibitory effect on H2-M, it has also been shown to modulate
460 the repertoire of peptides presented on MHCII with a mechanism still unclear (Denzin et al., 2005;
461 Karlsson 2005). Different ratios of H2-M and H2-O could thus distinguish the peptides sent out from
462 the early peripheral MIICs from those originating from the late perinuclear MIIC.
463
464 Using TEM, we found that the early peripheral antigen vesicles showed highly diverse morphologies
465 (Fig. 1F, left; Supplementary Fig. 1A). We detected various membrane structures harboring
466 intralumenal vesicles, consistent with the reports characterizing MIICs with multivesicular features
467 (Roche and Furuta, 2015; Unanue et al., 2016; van Lith et al., 2001; Xiu et al., 2011). The shapes
468 ranged from spherical to network-like or multilobular structures. However, also antigen-containing
469 single-membrane vesicles with round or horse-shoe shapes were detected. It has been shown in
470 dendritic cells, that intralumenal vesicles are not required for MHCII loading (Bosch et al., 2013). In
471 the other end of the range, also multilamellar MIIC have been reported (Unanue et al., 2016). These
472 notions suggest that MIIC function is not bound to certain vesicle morphology. Based on both the
473 morphological and vesicle marker-based heterogeneity, we propose that early peripheral antigen
474 vesicles are functional MIIC in transit. Antigen-containing vesicles can part off and fuse again or
475 migrate as such to the perinuclear region for gradual maturation, but our data suggests that the vesicles
476 could maintain the MIIC function throughout this pathway.
477
478 **Acknowledgements**
479 We are thankful for Laura Grönfors and Mervi Lindman for technical assistance. Microscopy and
480 flow cytometry were performed at the Cell Imaging and Cytometry (CIC) at the Turku Bioscience,
481 Turku, Finland and we thank the personnel, as well as the personnel of Turku Bioimaging, for their
482 generous help and expertise. Biocenter Finland is acknowledged for providing the imaging
483 infrastructures in CIC and in the Institute of Biotechnology, Helsinki. We thank Tampere Imaging

Facility for sharing their image analysis resources. Prof. Johanna Ivaska and Dr. Pranshu Sahgal are acknowledged for their help and generosity regarding reagents and protocols, and Prof. Johanna Ivaska and Prof. Ari Helenius for constructive discussions. Juan Palacios-Ortega is acknowledged for help in manuscript formatting.

**Funding**

This work was supported by the Academy of Finland (grant ID: 25700, 296684 and 307313; to P.K.M.), Sigrid Juselius and Jane and Aatos Erkko foundations (to P.K.M.), Turku doctoral programme in molecular medicine (TuDMM) (to M.V., S.H-P. and L.O.A.), Turku University foundation (to M.V., L.O.A.), and Paulo foundation (to E.K.).

**Competing interests**

No competing interests declared.

**Author contributions**

M.V., S.H-P., E.K., E.J., H.V., and P.K.M. conceived and designed the analysis.

M.V., S.H-P., E.K., V.P., P.P., and S.F. collected the data.

M.V., S.H-P., V.S., E.K., A.V.S., E.J., H.V., A.B., and P.K.M. contributed or performed the data analysis. A.B. developed the Matlab script and analysed data.

L.O.A. generated reagents.

M.V., S.H-P., A.V.S., and P.P. visualized the data.

P.K.M. and S.H-P. wrote the paper.

507 **Materials and Methods**

508 *Table 1. Key resources/reagents table*

| | Reagents | Source/Brand | Cat. number | Dilution or concentration | Use |
|---|---|---|---|---|---|
| **Antigens** | Anti-IgM-biotin | SouthernBiotech | 1021-08 | 10ug/ml | Antigen internalisation (FACS) |
| | 6nm Gold rat anti-mouse IgM | Jackson ImmunoResearch | 115-195-075 | | EM |
| | Rhodamine Red-X-AffiniPure Donkey anti-mouse IgM | JIR | 715-295-140 | 10ug/ml | IF/Live imaging |
| | Alexa Fluor 647AffiniPure Donkey anti-mouse IgM | JIR | 715-605-140 | 10ug/ml | IF/Live imaging |
| | Alexa Fluor 488 AffiniPure F(ab´)2 Fragment Donkey anti-mouse IgM | JIR | 715-546-020 | 10 µg/ml | Live imaging |
| | Donkey anti-mouse IgM AlexaFluor647-biotin | In-house | 715-605-140 + Thermo 21343 | 10ug/ml | IF |
| | HEL-biotin | In-house | Sigma-aldrich # L6876+ Thermo 21338 | | For DQ-Ova probe/FACS |
| **Antibodies** | Anti-Rab5 | CST | 3547 | 1:150 | IF |
| | Anti-Rab6 | CST | 9625S | 1:200 | IF |
| | Anti-Rab7 | Santa Cruz | Sc-376362 | 1:100 | IF |
| | Anti-Rab9 | CST | 5118 | 1:150 | IF |
| | Anti-Rab11 | CST | 5589 | 1:200 | IF |
| | Anti-EEA1 | Santa Cruz | Sc-6415 | 1:50 | IF |
| | Anti-LAMP1 | DSHB | 1D4B | 1:75 | IF |
| | Anti-CathepsinS | LSbio | B2550 | 1:50 | IF |
| | Anti-CathepsinS | Santa Cruz | sc-271619 | 1:50 | IF |
| | Anti-MHCII | Santa Cruz | Sc-59322 | 1:50 | IF |
| | Anti-MHCII-AF488 | In-house | Sc-59322 + Thermo A20000 | 1:50 | IF/Live imaging |
| | Anti-PCM1-AF647 | Santa Cruz | Sc-398365 AF647 | 1:200 | IF |
| | Donkey-anti-rabbit IgG (H+L) AlexaFluor 488/555/647 | Thermo | A21206, A31572, A31573 | 1:500 | IF |
| | Donkey anti-goat IgG (H+L) AlexaFluor 488/555 | Thermo | A11055, A21432 | 1:500 | IF |
| | Mouse anti-rat IgG Fcy Fragment Specific AlexaFluor 488/RRx/647 | JIR | 212-545-104 212-295-104 212-605-104 | 1:500 | IF |
| | Goat-anti-mouse IgG Fcy subclass 1 AlexaFluor 488/RRx/647 | JIR | 115-545-205 115-295-205 115-605-205 | 1:500 | IF |
| **Other** | LysoTracker Deep Red | Thermo | L12492 | 125 nM | Live imaging |
| | DQ-OVA-biotin | In-house | Thermo D12053 +EZ-Link Maleimide-PEG2-biotin (Thermo 21901BID) | 1:10 | FACS |
| | Fibronectin | Sigma | F4759-2MG | 4 µg/ml | IF |

509

510 *Cells and mice*

511 A20 mouse lymphoma cells stably expressing a hen egg lysozyme (HEL)–specific IgM BCR (D1.3)
512 (Williams et al, 1994) were maintained in complete RPMI (cRPMI; RPMI 1640 with 2.05 mM L-
513 glutamine supplemented with 10% fetal calf serum (FCS), 50 μM β-mercaptoethanol, 4 mM L-
514 glutamine, 10 mM HEPES and 100 U/ml Penicillin/Streptomycin). Primary splenic B cells were
515 isolated from MD4 mice (C57BL/6-Tg(IghelMD4)4Ccg/J, The Jackson Laboratory) using a negative
516 selection kit (StemCell Technologies, # 19854).

517

518 *Transfection*

519 A20 D1.3 cells were transfected as previously described (Sustar et al., 2018). Briefly, 2 million cells
520 were resuspended in 180ul of 2S transfection buffer (5 mM KCl, 15 mM MgCl2, 15 mM HEPES, 50
521 mM Sodium Succinate, 180 mM Na2HPO4/ NaH2PO4 pH 7.2) containing 2 μg of plasmid and
522 electroporated using AMAXA electroporation machine (program X-005, Biosystem) in 0.2 cm gap
523 electroporation cuvettes. Cells were then transferred to 2ml of cRPMI to recover overnight. Rab5a-
524 GFP plasmid was a kind gift from Prof. Johanna Ivaska.

525

526 *B cell activation and visualization of antigen vesicles by immunofluorescence*

527 A20 D1.3 or isolated primary B cells were activated with 10μg/ml of Alexa Fluor-647 or Rhodamine
528 Red-X (RRx) anti-mouse IgM (α-IgM) (Jackson ImmunoResearch), unless indicated otherwise. Cells
529 were labelled with fluorescently-labelled α -IgM for 10 min on ice, washed with PBS to remove
530 excess unbound antigen and resuspend in Imaging Buffer (PBS, 10% FCS). When indicated, cells
531 were also labelled with anti-MHCII-Alexa Fluor 488 on ice. After washing, cells were activated for
532 different timepoints in an incubator (5% $CO_2$, 37ºC) in a 12-wells PTFE diagnostic slide (Thermo,
533 #10028210), coated with fibronectin, and fixed with 4% PFA 10min at RT. Samples were blocked
534 and permeabilized with blocking buffer (5% horse or donkey serum, 0.3% Triton X100 in PBS) for
535 20min at RT. After blocking, samples were stained with primary antibodies for 1h at RT or 4ºC O/N
536 in staining buffer (1% BSA, 0.3% Triton X100 in PBS), followed by washes with PBS and incubation
537 with the secondary antibodies 30min at RT in PBS. Samples were mounted using FluoroMount-G
538 containing DAPI (Thermo #00495952).

539

540 *Visualization of antigen vesicles by live imaging*

541 A20 D1.3 cells (1 million/ml) were labelled with 125 nM LysoTracker Deep Red (Thermo # L12492)
542 for 1 hour in an incubator (5% $CO_2$, 37ºC), washed with PBS and resuspended in cRPMI. Cells were
543 then labelled with 10μg/ml of donkey anti-mouse IgM-AF488 on ice for 10 min and washed with

544 cold PBS. For surface-MHCII internalisation experiments, cells were stained on ice with anti-MHCII-
545 AF488 and 10µl/ml donkey-anti-mouse IgM-RRx for 5min and washed with cold PBS. Cells were
546 resuspended in cold Imaging Buffer and seeded on 4-well MatTek dishes on ice. After seeding, cells
547 were activated at 37 ºC inside the environmental chamber of the microscope and image immediately.
548
549 *Image acquisition and processing, spinning disk confocal microscopy*
550 Images were acquired using a 3i CSU-W1 spinning disk equipped with 405, 488, 561 and 640 nm
551 laser lines and 510-540, 580-654 and 672-712 nm filters and 63x Zeiss Plan-Apochromat objective.
552 Hamamatsu sCMOS Orca Flash4 v2 C11440-22CU (2048 x 2048 pixels, 1x1 binning) was used to
553 image fixed samples unless otherwise indicated, and Photometrics Evolve 10 MHz Back Illuminated
554 EMCCD (512 x 512 pixels, 1x1 binning) camera was used to image live samples.
555 All SDCM images were deconvolved with Huygens Essential version 16.10 (Scientific Volume
556 Imaging, The Netherlands, http://svi.nl), using the CMLE algorithm, with Signal to Noise Ratio of
557 20 and 40 iterations. For SRRF, 20-50 images were acquired from one single plane using timelapse
558 mode and processed in Fiji ImageJ using the SRRF module.
559
560 *Colocalisation analysis*
561 Colocalisation on Spinning Disk Confocal Microscope images were analysed with Huygens Essential
562 version 16.10 (Scientific Volume Imaging, The Netherlands, http://svi.nl), using optimized,
563 automatic thresholding. Colocalisation on SRRF images was performed on ImageJ using
564 Colocalisation Threshold tool. Graphs and statistics were prepared on GraphPad Prism (GraphPad
565 Software, La Jolla California USA).
566
567 *Analysis of antigen clustering*
568 Cluster analysis of the deconvolved data was done by batch processing in Matlab R2017a (The
569 MathWorks Inc.). Binary masks were created from full volumes containing one cell using the method
570 by Otsu. Objects were then segmented in 3D using the regionprops function. Only objects inside a
571 circular mask were kept in order to exclude clusters from adjacent cells, for simplicity this was done
572 in 2D by manually overlaying the image with a circle. The MTOC channel was segmented in the
573 same way and the cluster with the highest intensity value was identified as MTOC. The distances of
574 each cluster to the MTOC was calculated from the centroid positions in 3D. Graphs and statistics
575 were prepared on GraphPad Prism.
576
577

578 *Structured illumination microscopy (SIM)*
579 The samples were prepared as above in "*B cell activation and visualization of antigen vesicles by*
580 *immunofluorescence"* on fibronectin-coated MatTek dishes and mounted in Vectashield (Vector
581 Laboratories, US) mounting medium. 3D structured illumination (SIM) Imaging was performed with
582 GE Healthcare, DeltaVision OMX SR V4 with 60x/1.42 SIM Olympus Plan Apo N objective, front
583 Illuminated sCMOS cameras, 488, 568 and 640 nm solid-state lasers by optical sectioning of 0.125
584 µm. The SIM reconstruction was performed with OMX Acquisition software version 3.70. (GE
585 Healthcare, UK).
586
587 *Antigen internalisation for flow cytometry*
588 A20 D1.3 cells were stained on ice for 10 min with anti-IgM-biotin (Southern Biotech) or HEL-biotin
589 and washed with PBS. Cells were incubated at 37C and 5% CO2 at different timepoints. For time 0
590 the samples were kept on ice all the time After incubation, cells were kept on ice and stained with
591 streptavidin-633 (LifeTechonologies #S-21375) for 20min, washed and analysed. BD LSR Fortessa
592 analyser equipped with four lasers (405, 488, 561 and 640nm) was used.
593
594 *Antigen internalisation, immunofluorescence*
595 A20 D1.3 cells were stained on ice for 10 min with biotinylated anti-IgM-Alexa Fluor F647- (labelled
596 in-house) and washed with PBS. Cells were resuspended in Imaging Buffer (PBS, 10% FCS) and
597 activated for different timepoints in an incubator (5% CO2, 37ºC) on fibronectin-coated 12-well
598 microscope slide. After activation, slides were kept on ice to stop internalisation and stained with
599 streptavidin-Alexa Fluor 488 (#S11223) for 10 min. Cells were washed with PBS and fixed with 4%
600 PFA 10 min at RT. Samples were mounted using FluoroMount-G (Thermo 00-4958-02).
601
602 *DQ-Ova proteolysis reporter*
603 DQ Ovalbumin (Thermo Fisher Scientific D12053) was biotinylated in-house with EZ-Link
604 Maleimide-PEG2-biotin (Thermo 21901BID). HEL from (#L6876 Sigma) was biotinylated using
605 EZ-Link™ Sulfo-NHS-LC-LC-Biotin (Thermo 21338). A20 D1.3 cells were first incubated with
606 biotin-HEL or biotinylated anti-IgM (Southern Biotech) for 10 min on ice. After washing with PBS,
607 cells were incubated for 5min on ice with unlabelled streptavidin for IF samples or Alexa Fluor 633-
608 labelled streptavidin for flow cytometry samples, wash with PBS, and incubated 5min on ice with
609 biotinylated-DQ-Ova. After 3 washes with PBS, cells were activated in an incubator (5% CO2, 37ºC)
610 to allow internalisation of the probe-linked antigen. After the activation, cells were placed on ice and
611 analysed by flow cytometry immediately. For immunofluorescence samples, cells were activated on

612 12-well slides coated with fibronectin in the incubator, fixed with 4% PFA after activation, and
613 stained as previously described. DQ-Ova was excited with 488 nm laser and measured with filters
614 identical to Alexa Fluor 488 or GFP.
615
616 *Transmission electron microscopy*
617 A20 D1.3 cells were activated with a mixture of 6 nm colloidal-gold conjugated goat anti-Mouse IgM
618 (Jackson ImmunoResearch, 115-195-075; 1:650 dilution) and 20 µg/ml Alexa Fluor 647 labelled
619 donkey anti-mouse IgM F(ab')2 fragments (Jackson ImmunoResearch, 715-606-020) in imaging
620 buffer (0.5mM $CaCl_2$, 0.2mM $MgCl_2$, 5.5mM D-Glucose, 10% FBS in PBS) and placed on
621 fibronectin (4 µg/ml) coated glass coverslips (thickness #1) for 15 or 75 min. The cells were fixed
622 with 2 % Glutaraldehyde (EM-grade, Sigma G7651) in 0.1 M Na-Cacodylate buffer, pH 7.4, for 30
623 min at room temperature, and then washed twice for 3 min with 0.1 M Na-Cacodylate buffer, pH 7.4.
624 The samples were processed for TEM as described in Seemann et al., 2000. 60-nm-thick sections
625 parallel to the cover slip were cut using a Leica EM Ultracut UC7 ultramicrome (Leica Mikrosysteme
626 GmbH, Austria). The electron micrographs post-stained with uranyl acetate and lead citrate, and
627 imaged with Jeol JEM 1400 transmission electron microscope (Jeol Ltd., Tokyo, Japan) equipped
628 with a bottom mounted CCD-camera (Orius SC 1000B, Gatan Inc., Pleasanton, CA) and Jeol JEM-
629 1400 Plus equipped with OSIS Quemesa bottom-mounted CCD-Camera (EMSIS, Germany), both
630 operating at 80 kV.
631
632 *Statistical analysis*
633 Statistical significances were calculated using unpaired Student's *t*-test or two-way Anova. Statistical
634 values are denoted as: $*P<0.05$, $**P<0.01$, $***P<0.001$, $****P<0.0001$.
635
636 **References**
637
638 **Adler, L. N., Jiang, W., Bhamidipati, K., Millican, M., Macaubas, C., Hung, S. chen and Mellins, E. D.** (2017). The other function:
639 Class II-restricted antigen presentation by B cells. *Front. Immunol.*
640 **Aluvihare, V. R., Khamlichi, A. A., Williams, G. T., Adorini, L. and Neuberger, M. S.** (1997). Acceleration of intracellular
641 targeting of antigen by the B-cell antigen receptor: importance depends on the nature of the antigen-antibody interaction. *EMBO*
642 *J.* **16**, 3553–62.
643 **Amigorena, S., Drake, J. R., Webster, P. and Mellman, I.** (1994). Transient accumulation of new class II MHC molecules in a novel
644 endocytic compartment in B lymphocytes. *Nature* **369**, 113–20.
645 **Barroso, M., Tucker, H., Drake, L., Nichol, K. and Drake, J. R.** (2015). Antigen-B Cell Receptor Complexes Associate with
646 Intracellular major histocompatibility complex (MHC) Class II Molecules. *J. Biol. Chem.* **290**, 27101–12.
647 **Bosch, B., Heipertz, E. L., Drake, J. R. and Roche, P. A.** (2013). Major histocompatibility complex (MHC) class II-peptide

648 complexes arrive at the plasma membrane in cholesterol-rich microclusters. *J. Biol. Chem.*
649 **Castellino, F. and Germain, R. N.** (1995). Extensive trafficking of MHC class II-invariant chain complexes in the endocytic pathway
650 and appearance of peptide-loaded class II in multiple compartments. *Immunity* **2**, 73–88.
651 **Chen, K., Healy, M. D. and Collins, B. M.** (2019). Towards a molecular understanding of endosomal trafficking by Retromer and
652 Retriever. *Traffic*.
653 **Clotworthy, M. and Traynor, D.** (2006). On the effects of cycloheximide on cell motility and polarisation in Dictyostelium
654 discoideum. *BMC Cell Biol*. **7**, 5.
655 **Darvishi, E. and Woldemichael, G. M.** (2016). Cycloheximide Inhibits Actin Cytoskeletal Dynamics by Suppressing Signaling via
656 RhoA. *J. Cell. Biochem.*
657 **Davidson, H. W., West, M. A. and Watts, C.** (1990). Endocytosis, intracellular trafficking, and processing of membrane IgG and
658 monovalent antigen/membrane IgG complexes in B lymphocytes. *J. Immunol*. **144**, 4101–9.
659 **Delevoye, C., Marks, M. S. and Raposo, G.** (2019). Lysosome-related organelles as functional adaptations of the endolysosomal
660 system. *Curr. Opin. Cell Biol*. **59**, 147–158.
661 **Denzin, L. K., Fallas, J. L., Prendes, M. and Yi, W.** (2005). Right place, right time, right peptide: DO keeps DM focused. *Immunol.*
662 *Rev*.
663 **Gondré-Lewis, T. a, Moquin, a E. and Drake, J. R.** (2001). Prolonged antigen persistence within nonterminal late endocytic
664 compartments of antigen-specific B lymphocytes. *J. Immunol*. **166**, 6657–64.
665 **Gustafsson, N., Culley, S., Ashdown, G., Owen, D. M., Pereira, P. M. and Henriques, R.** (2016). Fast live-cell conventional
666 fluorophore nanoscopy with ImageJ through super-resolution radial fluctuations. *Nat. Commun.*
667 **Homma, Y., Kinoshita, R., Kuchitsu, Y., Wawro, P. S., Marubashi, S., Oguchi, M. E., Ishida, M., Fujita, N. and Fukuda, M.**
668 (2019). Comprehensive knockout analysis of the Rab family GTPases in epithelial cells. *J. Cell Biol.*
669 **Huotari, J. and Helenius, A.** (2011). Endosome maturation. *EMBO J*. **30**, 3481–500.
670 **Hutagalung, A. H. and Novick, P. J.** (2011). Role of Rab GTPases in membrane traffic and cell physiology. *Physiol. Rev*. **91**, 119–
671 49.
672 **Karlsson, L.** (2005). DM and DO shape the repertoire of peptide-MHC-class-II complexes. *Curr. Opin. Immunol.*
673 **Kirkham, M., Fujita, A., Chadda, R., Nixon, S. J., Kurzchalia, T. V., Sharma, D. K., Pagano, R. E., Hancock, J. F., Mayor, S.**
674 **and Parton, R. G.** (2005). Ultrastructural identification of uncoated caveolin-independent early endocytic vehicles. *J. Cell Biol.*
675 **168**, 465–476.
676 **Langemeyer, L., Bastos, R. N., Cai, Y., Itzen, A., Reinisch, K. M. and Barr, F. A.** (2014). Diversity and plasticity in Rab GTPase
677 nucleotide release mechanism has consequences for Rab activation and inactivation. *Elife*.
678 **Lankar, D., Vincent-Schneider, H., Briken, V., Yokozeki, T., Raposo, G. and Bonnerot, C.** (2002). Dynamics of major
679 histocompatibility complex class II compartments during B cell receptor-mediated cell activation. *J. Exp. Med*. **195**, 461–72.
680 **Manders, E. M.M. Verbeek, F. J. Aten, J. A.** (1993). Measurement of co-localization of objects in dual-colour confocal images. *J.*
681 *Microsc*. **169**, 375–382.
682 **Martinez-Martin, N., Maldonado, P., Gasparrini, F., Frederico, B., Aggarwal, S., Gaya, M., Tsui, C., Burbage, M., Keppler, S.**
683 **J., Montaner, B., et al.** (2017). A switch from canonical to noncanonical autophagy shapes B cell responses. *Science* **355**, 641–
684 647.
685 **Mellins, E. D. and Stern, L. J.** (2014). HLA-DM and HLA-DO, key regulators of MHC-II processing and presentation. *Curr. Opin.*
686 *Immunol*. **26**, 115–22.
687 **Oksvold, M. P., Pedersen, N. M., Forfang, L. and Smeland, E. B.** (2012). Effect of cycloheximide on epidermal growth factor
688 receptor trafficking and signaling. *FEBS Lett.*
689 **Paul, P., van den Hoorn, T., Jongsma, M. L. M., Bakker, M. J., Hengeveld, R., Janssen, L., Cresswell, P., Egan, D. a, van Ham,**
690 **M., Ten Brinke, A., et al.** (2011). A Genome-wide multidimensional RNAi screen reveals pathways controlling MHC class II
691 antigen presentation. *Cell* **145**, 268–83.

692 **Rink, J., Ghigo, E., Kalaidzidis, Y. and Zerial, M.** (2005). Rab conversion as a mechanism of progression from early to late
693 endosomes. *Cell* **122**, 735–49.
694 **Roche, P. A. and Furuta, K.** (2015). The ins and outs of MHC class II-mediated antigen processing and presentation. *Nat. Rev.*
695 *Immunol.* **15**, 203–16.
696 **Seemann, J., Jokitalo, E. J. and Warren, G.** (2000). The Role of the Tethering Proteins p115 and GM130 in Transport through the
697 Golgi Apparatus In Vivo. *Mol. Biol. Cell.*
698 **Siemasko, K., Eisfelder, B. J., Williamson, E., Kabak, S. and Clark, M. R.** (1998). Cutting edge: signals from the B lymphocyte
699 antigen receptor regulate MHC class II containing late endosomes. *J. Immunol.* **160**, 5203–8.
700 **Sustar, V., Vainio, M., & Mattila, P. K**. Visualization and Quantitative Analysis of the Actin Cytoskeleton Upon B Cell Activation. *B*
701 *Cell Receptor Signaling*, 243.
702 **Tsui, C., Martinez-Martin, N., Gaya, M., Maldonado, P., Llorian, M., Legrave, N. M., Rossi, M., MacRae, J. I., Cameron, A.**
703 **J., Parker, P. J., et al.** (2018). Protein Kinase C-β Dictates B Cell Fate by Regulating Mitochondrial Remodeling, Metabolic
704 Reprogramming, and Heme Biosynthesis. *Immunity* **48**, 1144-1159.e5.
705 **Unanue, E. R., Turk, V. and Neefjes, J.** (2016). Variations in MHC Class II Antigen Processing and Presentation in Health and
706 Disease. *Annu. Rev. Immunol.*
707 **van Lith, M., van Ham, M., Griekspoor, A., Tjin, E., Verwoerd, D., Calafat, J., Janssen, H., Reits, E., Pastoors, L. and Neefjes,**
708 **J.** (2001). Regulation of MHC Class II Antigen Presentation by Sorting of Recycling HLA-DM/DO and Class II within the
709 Multivesicular Body. *J. Immunol.* **167**, 884–892.
710 **Vascotto, F., Lankar, D., Faure-André, G., Vargas, P., Diaz, J., Le Roux, D., Yuseff, M.-I., Sibarita, J.-B., Boes, M., Raposo,**
711 **G., et al.** (2007a). The actin-based motor protein myosin II regulates MHC class II trafficking and BCR-driven antigen
712 presentation. *J. Cell Biol.* **176**, 1007–1019.
713 **Vascotto, F., Le Roux, D., Lankar, D., Faure-André, G., Vargas, P., Guermonprez, P. and Lennon-Duménil, A.-M.** (2007b).
714 Antigen presentation by B lymphocytes: how receptor signaling directs membrane trafficking. *Curr. Opin. Immunol.* **19**, 93–8.
715 **Vonderheit, A. and Helenius, A.** (2005). Rab7 associates with early endosomes to mediate sorting and transport of Semliki forest
716 virus to late endosomes. *PLoS Biol.*
717 **Wandinger-Ness, A. and Zerial, M.** (2014). Rab proteins and the compartmentalization of the endosomal system. *Cold Spring Harb.*
718 *Perspect. Biol.* **6**, a022616.
719 **West, M. A., Lucocq, J. M. and Watts, C.** (1994). Antigen processing and class II MHC peptide-loading compartments in human B-
720 lymphoblastoid cells. *Nature* **369**, 147–51.
721 **Whitmire, J. K., Asano, M. S., Kaech, S. M., Sarkar, S., Hannum, L. G., Shlomchik, M. J. and Ahmed, R.** (2009). Requirement
722 of B Cells for Generating CD4+ T Cell Memory. *J. Immunol.*
723 **Xiu, F., Côté, M.-H., Bourgeois-Daigneault, M.-C., Brunet, A., Gauvreau, M.-É., Shaw, A. and Thibodeau, J.** (2011). Cutting
724 edge: HLA-DO impairs the incorporation of HLA-DM into exosomes. *J. Immunol.* **187**, 1547–51.
725 **Yonemura, Y., Li, X., Müller, K., Krämer, A., Atigbire, P., Mentrup, T., Feuerhake, T., Kroll, T., Shomron, O., Nohl, R., et al.**
726 (2016). Inhibition of cargo export at ER exit sites and the trans-Golgi network by the secretion inhibitor FLI-06. *J. Cell Sci.*
727 **Yuseff, M.-I., Reversat, A., Lankar, D., Diaz, J., Fanget, I., Pierobon, P., Randrian, V., Larochette, N., Vascotto, F., Desdouets,**
728 **C., et al.** (2011). Polarized secretion of lysosomes at the B cell synapse couples antigen extraction to processing and presentation.
729 *Immunity* **35**, 361–74.
730

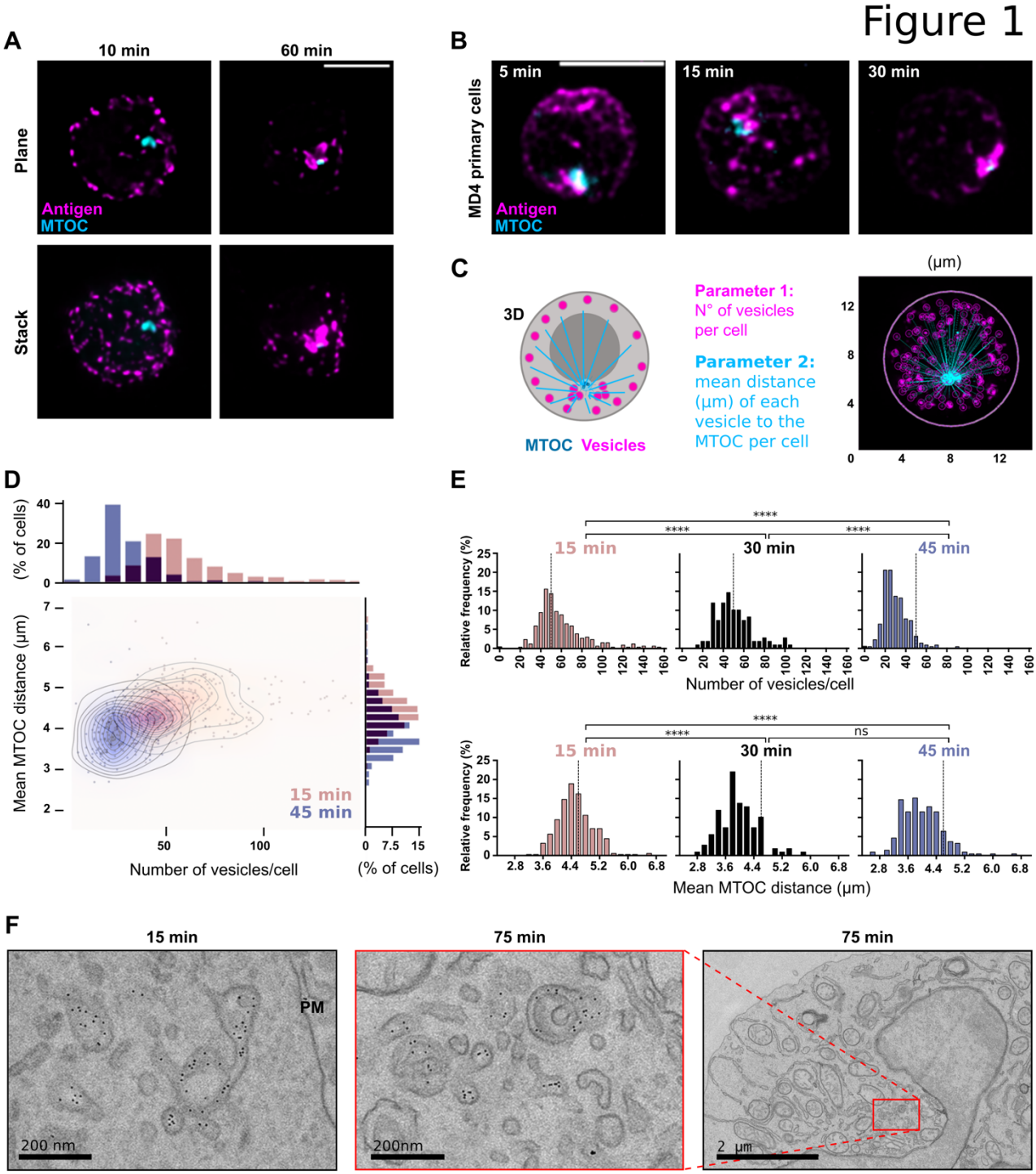


**Figure 1. Antigen vesicles traffic to a perinuclear compartment in the vicinity of the MTOC. A** A20 D1.3 B cells were activated with Alexa Fluor-labelled anti-IgM antibodies (AF-αIgM) (antigen, magenta) for 10 and 60 min and stained with antibodies against PCM-1 (MTOC, cyan). 3D SDCM was performed and the images were deconvolved using Huygens software. Upper panel shows single confocal planes and the lower panel shows z-projections of the whole stacks of representative cells. Scale bar 5 µm. **B** Primary MD4 B cells were activated with AF-αIgM (antigen, magenta) for different timepoints and stained with antibodies against PCM-1 (MTOC, cyan). 3D SDCM was performed and the images were deconvolved using Huygens software. Z-projections of the whole stacks from representative cells are shown. Scale bar 5 µm. **C** A schematic of the vesicle quantification using a MatLab-based script. Number of antigen vesicles in one cell (in magenta) and mean distance from all the vesicles to the MTOC (in cyan) is measured in a 3D image. Left, schematic representation; right, example image from the script. **D** Quantification of data in A. 3D images from cells activated for 15 (pink) and 45 (blue) min were analysed as in C. Upper axis shows mean number of vesicles per cell and right axis shows mean distance of the vesicles to MTOC per cell. The two timepoints were compared using a density plot. **E** Comparison of samples prepared as in A, activated for 15, 30 and 45 min and analysed as in C and D. Dashed line represent the median of the cell population in 15 min. Statistical analysis was done using Student's t-test. Timepoints 15 and 45 min contain 2 experiments, n>200 cells; and timepoint of 30 min is derived from one experiment, n>100 cells. **F** A20 D1.3 cells were activated with αIgM conjugated with 6nm colloidal gold particles mixed with AF647-αIgM, for 15 and 75 min and imaged using Transmission Electron Microscopy. PM – Plasma membrane. Scale bars 200 nm and 2 µm.

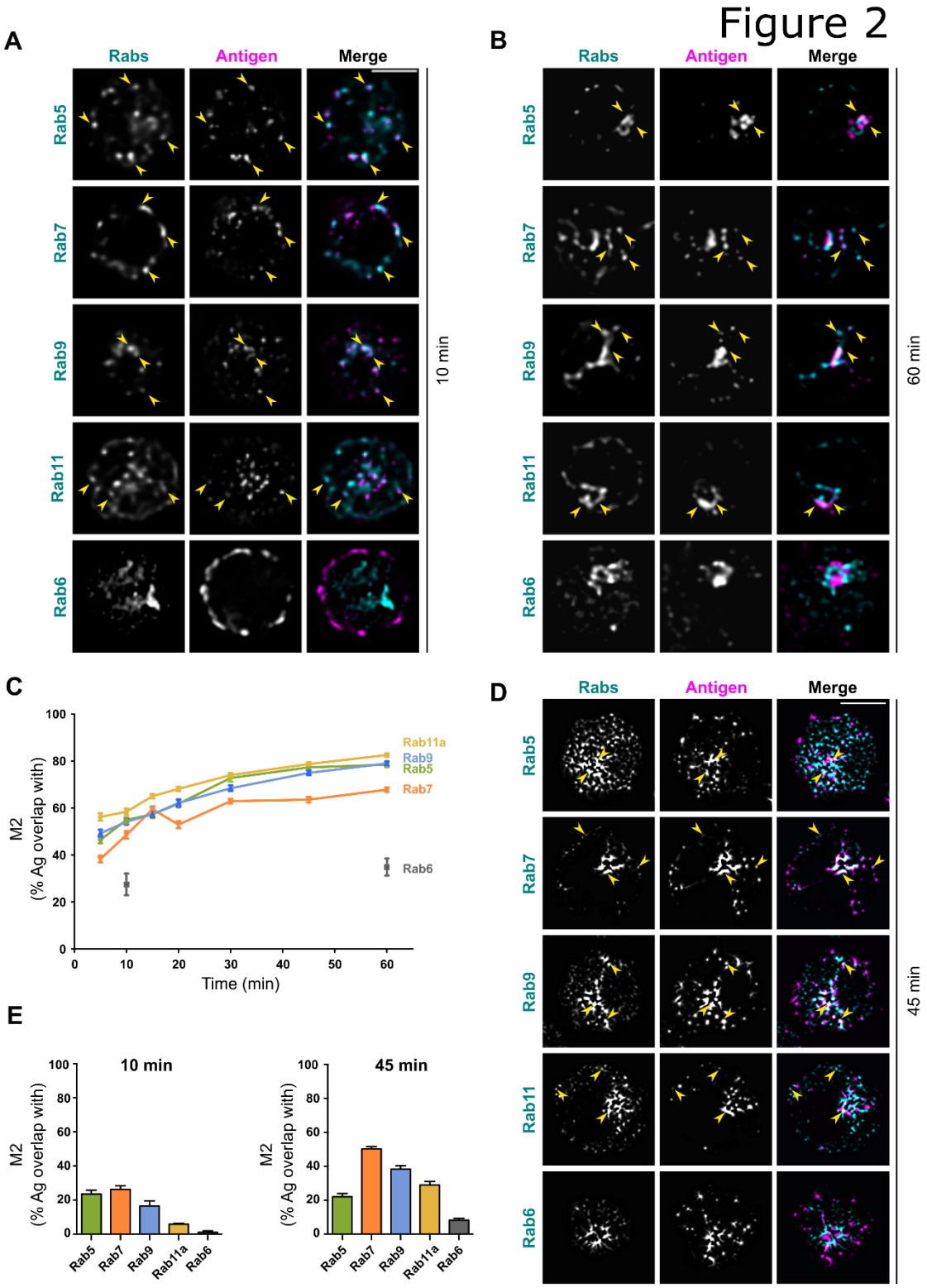


**Figure 2. Colocalisation analysis of antigen with different Rab-proteins. A-B** SDCM imaging of A20 D1.3 cells activated with AF647-αIgM (antigen, magenta) for 10 min **(A)** or 60 min **(B)** and immunostained for different Rab-proteins: Rab5, Rab7, Rab9, Rab11 and Rab6 (cyan). Images were deconvolved with Huygens software. Single confocal planes from representative cells are shown and examples of colocalising vesicles are pointed to with yellow arrow-heads. See Supplementary Figure 3A-B for z-projections. Scale bar 5 µm. **C** Quantification of the data in A and B with additional timepoints. Antigen colocalisation with different Rab-proteins was measured from deconvolved images by analysing Manders´ overlap coefficients using Huygens. Data from three independent experiments (>80 cells/timepoint). Results are shown as mean ±SEM. **D** Samples were prepared with cells activated for 10 or 45 min as in A-B and imaged with iterative imaging of a single plane with SDCM (20-25 frames/plane) and post-processed to obtain SRRF super-resolution image (antigen, magenta; Rabs, cyan). Examples of colocalising vesicles are pointed to with yellow arrowheads. Scale bar 5 µm. **E** Quantification of the SRRF data in D by analysing Manders´ overlap coefficients with ImageJ. Data in 45 min timepoint is from two independent experiments and 10 min from one experiment (>25 cells / timepoint). Results are shown as mean ±SEM.

Figure 3

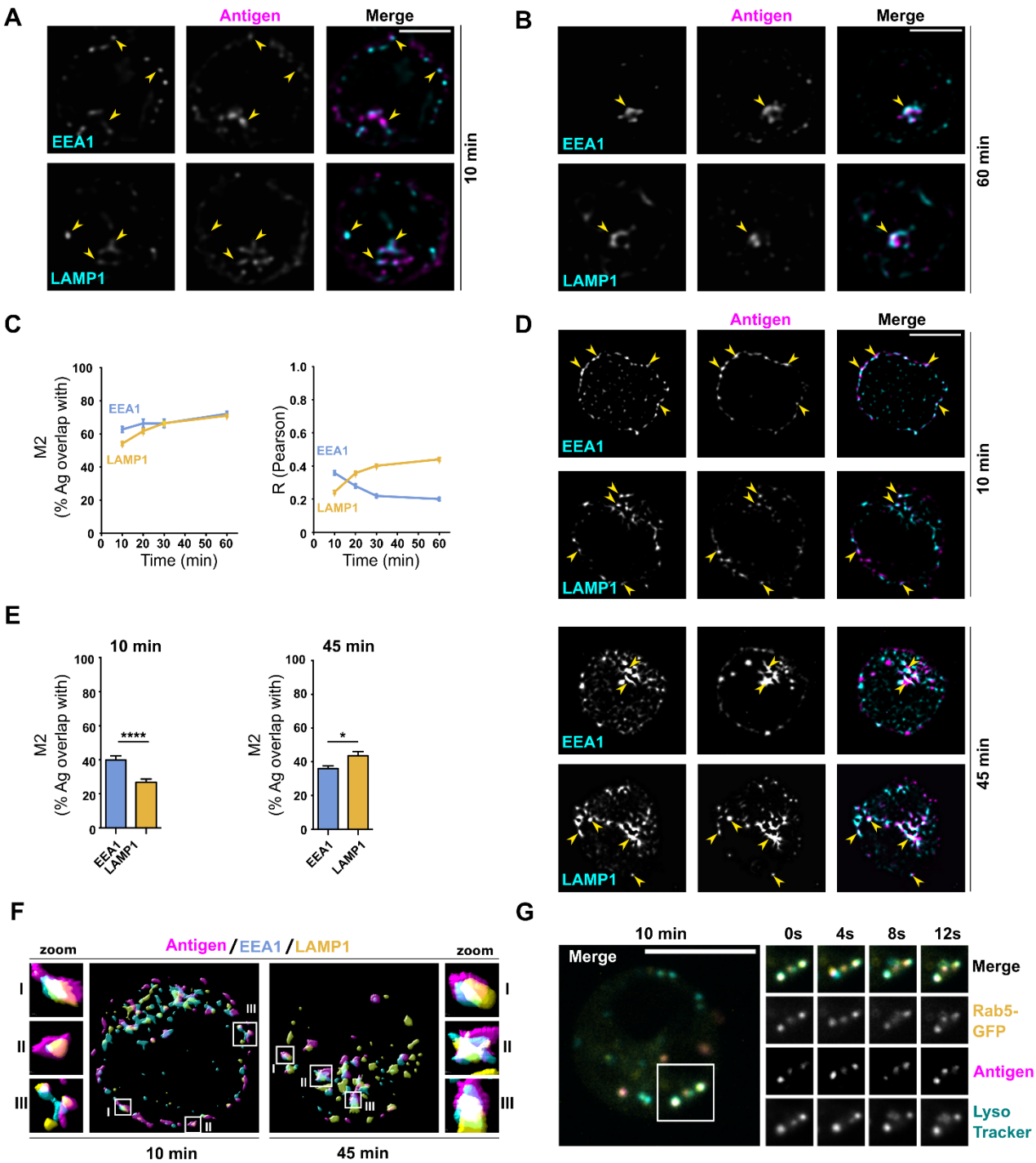


**Figure 3. Antigen colocalises with both EEA1 and LAMP1 while trafficking to the perinuclear region. A-B** SDCM imaging of A20 D1.3 cells activated with AF647-αIgM (antigen, magenta) for 10 min **(A)** or 60 min **(B)** and immunostained for EEA1 or LAMP1 (cyan). Images were deconvolved with Huygens software. Single confocal planes from representative cells are shown and examples of colocalising vesicles are pointed to with yellow arrow-heads. See Supplementary Figure 3C-D for z-projections. Scale bar 5 µm. **C** Quantification of the data in A and B with additional timepoints. Antigen colocalisation with EEA1 and LAMP1 was measured from deconvolved images by analysing Manders´ overlap coefficients and Pearson´s correlation coefficients using Huygens. Data from two independent experiments with >40 cells / timepoint. Results are shown as mean ±SEM. **D** Samples were prepared with cells activated for 10 or 45 min as in A-B and imaged with iterative imaging of a single plane with SDCM (20-25 frames/plane) and post-processed to obtain SRRF super-resolution image (antigen, magenta; EEA/LAMP1, cyan). Examples of colocalising vesicles are pointed to with yellow arrowheads. Scale bar 5 µm. **E** Quantification of the SRRF data in D by analysing Manders´ overlap coefficients with ImageJ. Data from three independent experiments (>30 cells/timepoint). Results are shown as mean ±SEM. **F** Surface reconstruction using Huygens rendering tool of SRRF images from samples prepared as in D (antigen, magenta) and immunostained for EEA1 (cyan) and LAMP1 (yellow). Three selected example vesicles are highlighted by zoom-in. **G** A20 D1.3 cells were transfected with GFP-Rab5 (yellow), loaded with LysoTracker (LT; cyan) and activated with RRx-αIgM (antigen, magenta). Live-imaging was performed with SDCM (ORCA camera) on a single plane. On the left, a merge image of a representative cell after 10 min of activation is shown. On the right, the region in the white square is followed in split channels as a timelapse for 12 sec, starting 10 min after activation. See supplementary Movie 1.

Figure 4

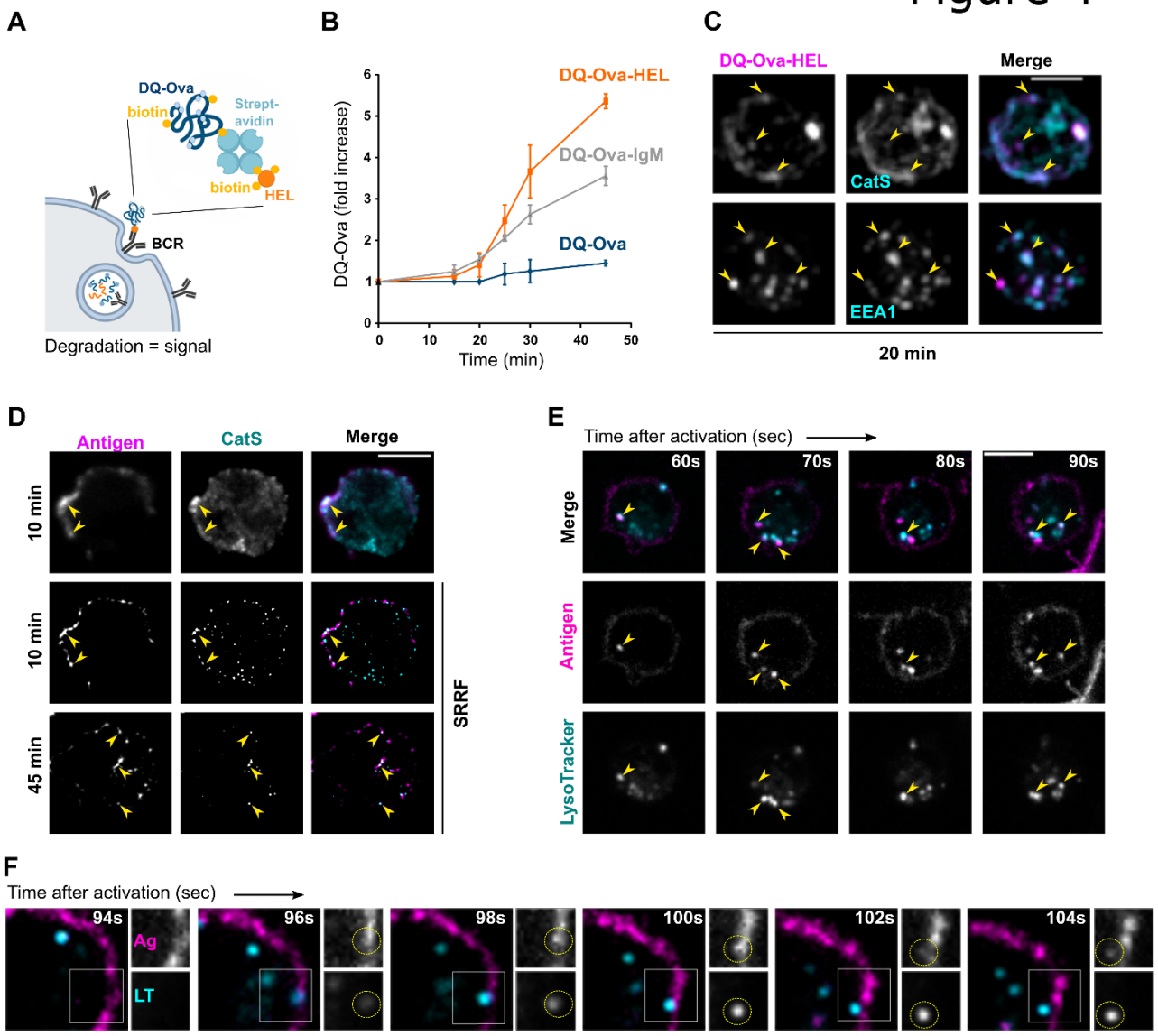


**Figure 4. Internalised antigen incorporates into vesicles with low pH and capability to degrade cargo. A** Schematic view of preparing DQ-Ova-antigen (HEL) sandwich to probe proteolysis of antigen internalised by the BCR. **B** DQ-Ova and DQ-Ova-antigen (αIgM or HEL) degradation assessed by flow cytometry. Cells were labelled as in A, washed, and incubated for different timepoints at 37ºC and fluorescence of DQ-OVA was acquired immediately. Results are shown as fold increase (mean ±SD of the DQ-OVA intensity, normalized to the intensity at time zero). N>2 independent experiments. **C** A20 D1.3 cells activated with DQ-Ova-HEL (magenta) as in B, for 20 min, were immunostained for EEA1 or CatS (cyan). Images were acquired using SDCM with EVOLVE (EMCCD) camera. Z-projections of representative cells (n = 3 independent experiments) are shown with examples of colocalising vesicles pointed to with yellow arrow-heads. Scale bar 5 µm. **D** A20 D1.3 cells activated with AF647-αIgM (antigen, magenta) for 10 or 45 min and immunostained for CatS (cyan) were imaged with conventional SDCM (upper panel, single plane) or with iterative imaging to obtain SRRF super-resolution image (20-25 frames/plane) (middle and bottom panels). Examples of colocalising vesicles are pointed to with yellow arrowheads. Scale bar 5 µm. **E-F** A20 D1.3 were loaded with LysoTracker (cyan) and activated with AF488 F(ab´)2-αIgM (antigen, magenta). Live-imaging was performed with SDCM with EVOLVE (EMCCD) camera every 2s (E) or 500 ms (F), starting as soon as possible after transition of the cells to 37°C under the microscope. **(E)** A timelapse from a representative cell is shown and examples of colocalising vesicles are pointed to with yellow arrowheads. Scale bar 5 µm. See supplementary Movie 2. **(F)** A timelapse of an example movie highlighting a probable fusion event between an internalising antigen vesicle and a LT vesicle (dashed yellow circle). A white square in the merge image (left) depicts the region of the split channel insets. See supplementary Movie 3.

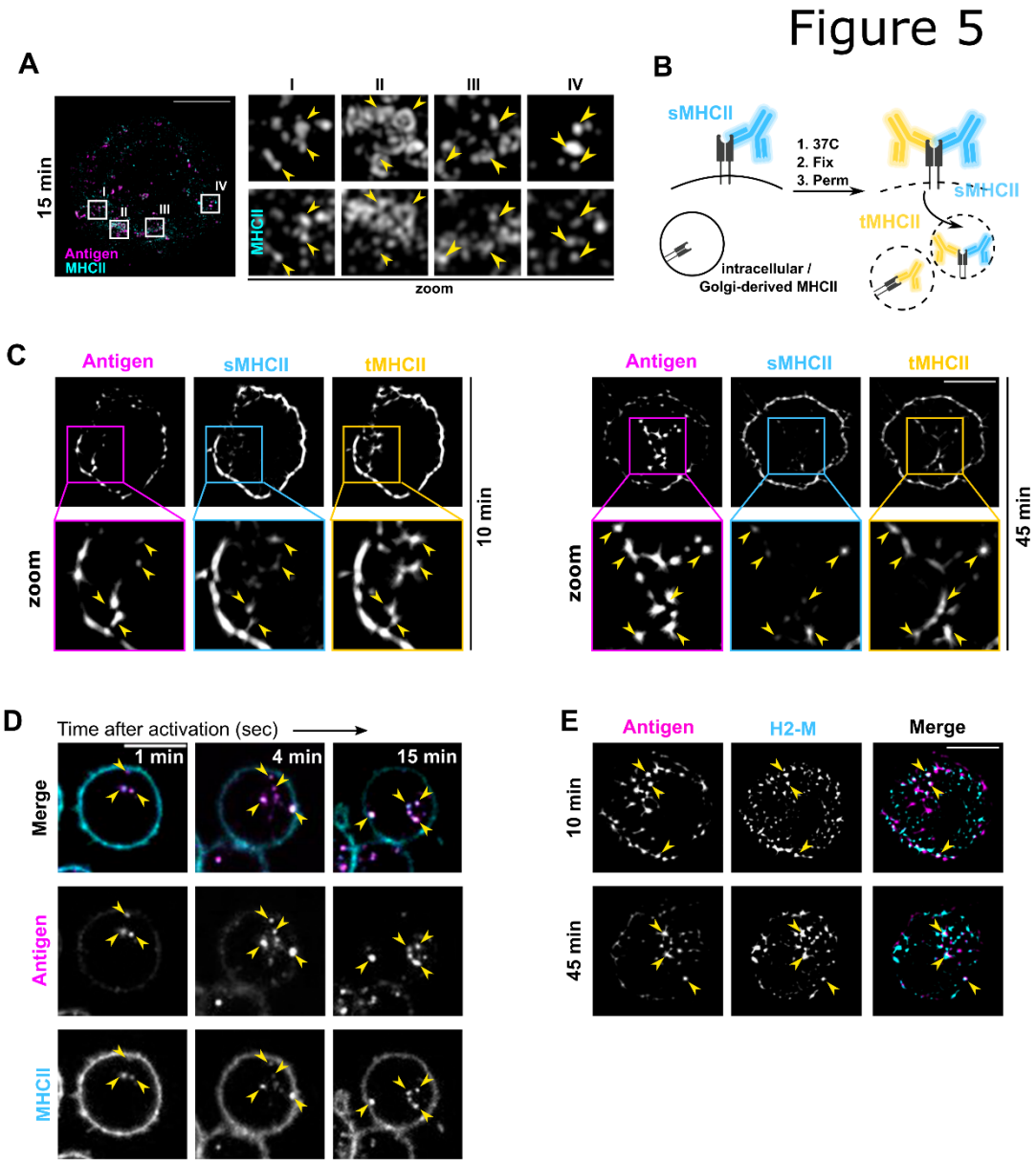


**Figure 5. Antigen and surface-derived MHCII rapidly converge after internalisation. A** SIM imaging of A20 D1.3 cells activated with AF647-αIgM (antigen, magenta) for 15 min and immunostained for MHC-II (cyan). A representative cell (stack image; 0.125 µm strep size) is shown on the left with white squares indicating insets I-IV shown on panel on the right. Scale bar 5 µm. **B** A schematic view on the staining to distinguish surface-derived MHCII from the total pool, used in C-D. **C** A20 D1.3 cells (plane image; antigen in magenta) were stained with anti-MHCII antibodies (AF488) before activation with RRx-αIgM (antigen, magenta) to labelling surface-bound MHCII (sMHCII in cyan). After activation of 10 or 45 min at 37ºC, cells were fixed and permeabilised to stain with anti-MHCII antibody and a secondary antibody (AF633; tMHCII, yellow). Samples were imaged with iterative imaging of a single plane with SDCM (20-25 frames/plane) and post-processed to obtain SRRF super-resolution image. The panel on top shows a representative cell with white square depicting the region for the zoom-in in the lower panel. Examples of colocalising vesicles are pointed to with yellow arrowheads. Scale bar 5um. **D** Live imaging of A20D1.3 stained on ice with AF488-anti-MHCII antibodies (cyan) and RRx-αIgM (antigen, magenta). Samples were imaged every 5 seconds using SDCM after 1 min at 37 °C (ORCA camera). A timelapse from a representative cell is shown and examples of colocalising vesicles are pointed to with yellow arrowheads. Scale bar 5 µm. See supplementary Movie 4. **E** SRRF imaging of A20 D1.3 cells activated with AF647-αIgM (antigen, magenta) for 10 or 45 min and immunostained for H2-M (cyan). A representative cell is shown and examples of colocalising vesicles are pointed to with yellow arrow-heads. Scale bar 5 µm.

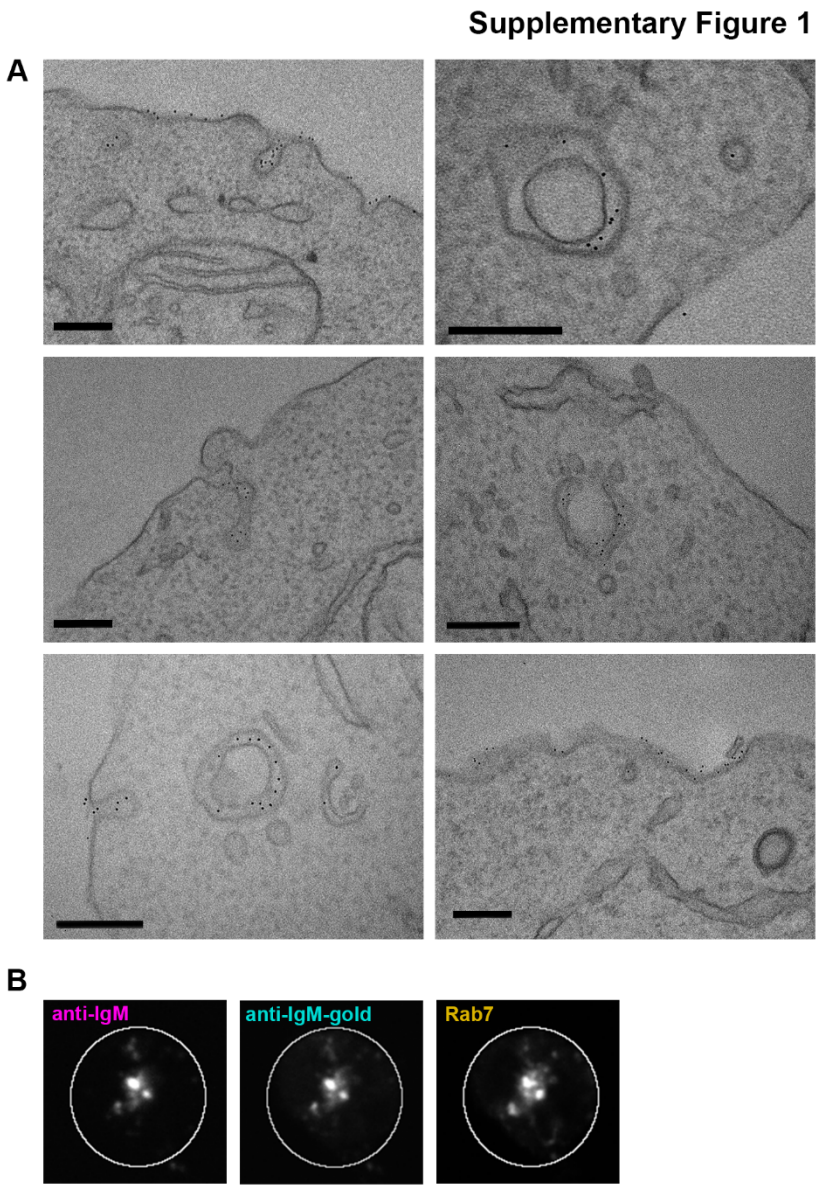


811

812 **Supplementary Figure S1. A** A20 D1.3 cells were activated with αIgM conjugated with 6nm
813 colloidal gold particles mixed with AF647-αIgM, for 15 min and imaged using Transmission
814 Electron Microscopy. Scale bars 200 nm. **B** The localization of colloidal gold-conjugated αIgM
815 was controlled by immunofluorescence analysis of sample duplicates (from A). The cells activated
816 for 75 min were fixed and permeabilised, and gold-conjugated αIgM was stained using an isotype-
817 secondary antibody (cyan) and compared to AF647-αIgM. The cells were also immunostained with
818 anti-Rab7 antibody (yellow). SDCM image shows single section of a representative cell (cell
819 plasma membrane marked with a white circle).

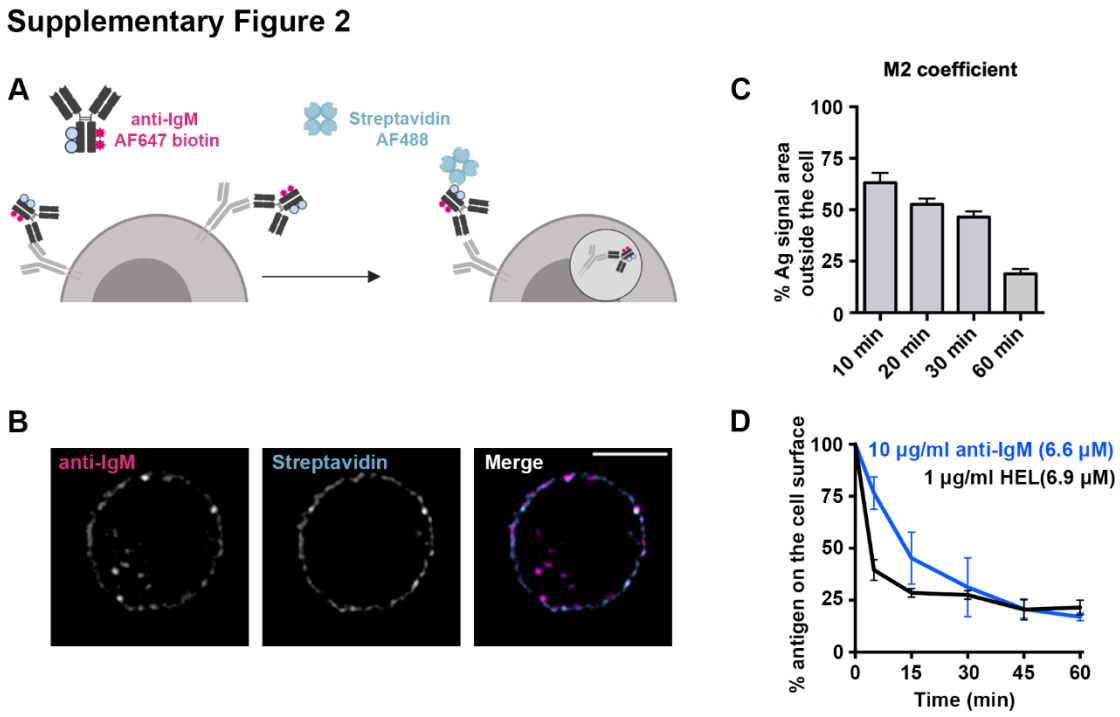


**Supplementary Figure S2. A** Schematic representation of the staining to distinguish between internalised AF647-αIgM (magenta) and surface-resident αIgM (probed with AF488-streptavidin; cyan). **B** SDCM imaging of A20 D1.3 cells activated with biotin-AF647-αIgM for 10 min. AF647-αIgM used for activation is shown in magenta, and surface-resident αIgM (AF488-streptavidin) in cyan. SDCM images were deconvolved with Huygens software. Single confocal plane from a representative cell is presented. Scale bar 5 µm. **C** Quantification of the data in B, including additional timepoints. 3D images from cells activated for 10, 20, 30 and 60 minutes were analysed for Manders´ overlap coefficients (M2) using ImageJ. Data shown as mean ±SEM of one experiment (n>20 cells per timepoint). **D** A20 D1.3 cells labelled with biotinylated-αIgM or biotinylated-HEL were incubated at 37 ºC at different timepoints and stained on ice with AF488-streptavidin to detect surface-resident αIgM. Intensity was normalised to time 0 (100%). Data from at least three independent experiments is presented as mean ±SD.

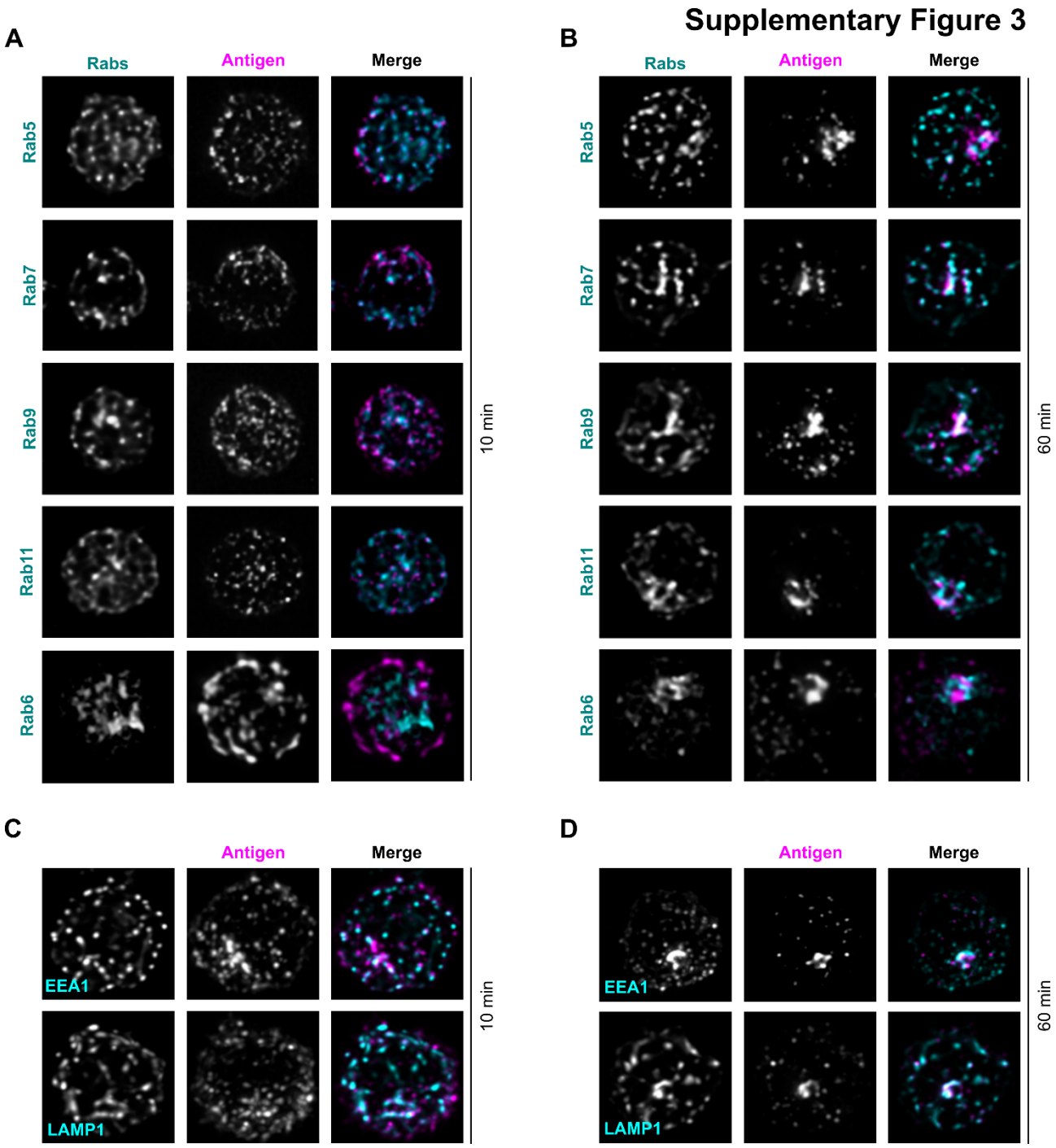


**Supplementary Figure S3. Colocalization of antigen with different Rab-proteins. A-B** SDCM imaging of A20 D1.3 cells activated with AF647-αIgM (antigen, magenta) for 10 min **(A)** or 60 min **(B)** and immunostained for different Rab-proteins: Rab5, Rab7, Rab9, Rab11 and Rab6 (cyan). Images were deconvolved with Huygens software. Z-projections of the 3D images from representative cells are shown. **C-D** SDCM imaging of A20 D1.3 cells activated with AF647-αIgM (antigen, magenta) for 10 min **(C)** or 60 min **(D)** and immunostained for EEA1 or LAMP1 (cyan). Images were deconvolved with Huygens software. Z-projections of the 3D images from representative cells are shown.

## Supplementary Figure 4

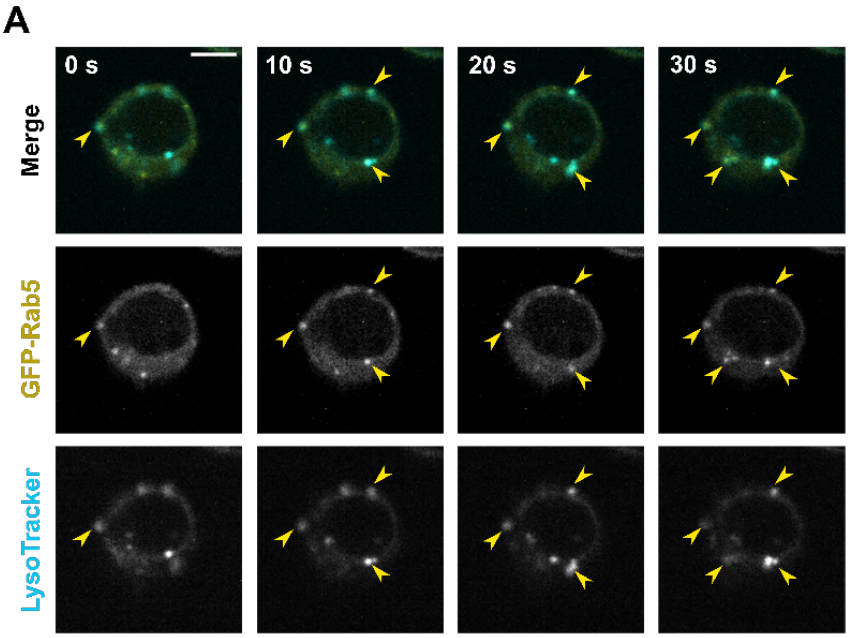


842

843 **Supplementary Figure S4. Rab5-GFP localises to LysoTracker-positive vesicles already**
844 **before activation. A.** A20 D1.3 cells were transfected with GFP-Rab5 (yellow) and loaded with
845 LysoTracker (LT; cyan). Live-imaging was performed with SDCM (with sCMOS Orca Flash4 v2
846 camera) on a single plane. On the upper panel, a merge image of a representative cell is shown as a
847 timelapse for 30 seconds. Split channels for GFP-Rab5 and LysoTracker are shown in the middle
848 and bottom panel respectively. Examples of colocalizing vesicles pointed to with yellow arrow-
849 heads. Scale bar 5 µm.

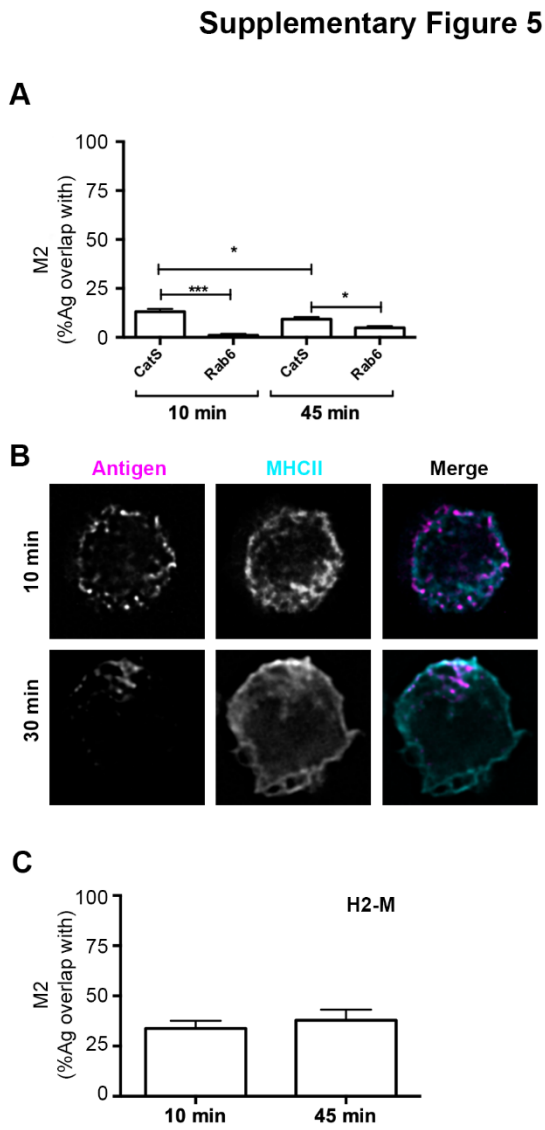


**Supplementary Figure S5. A** Quantification of the data shown in Fig. 4D. Antigen colocalization with CatS was measured from SRRF images by analysing Manders´ overlap coefficients using ImageJ. Data from two independent experiments (>30 cells/timepoint). Results are shown as mean ±SEM. **B** A20 D1.3 cells were activated with AF647-αIgM (antigen in magenta) for 10 or 30 minutes. Samples were then fixed, permeabilised and stained with anti-MHCII (cyan). SDCM images were deconvolved with Huygens software. Single confocal sections from representative cells are shown. **C** Quantification of the data shown in Fig. 5E. Antigen colocalization with H2-M was measured from SRRF images by analysing Manders´ overlap coefficients using ImageJ. Data from two independent experiments (>30 cells/timepoint). Results are shown as mean ±SEM.

860 **Supplementary Movie 1. Antigen is transported in vesicles positive for early and late**
861 **endosomal markers.** A20 D1.3 cells were transfected with GFP-Rab5 (right panel), loaded with
862 LysoTracker (left panel) and activated with RRx-αIgM (middle panel). Live-imaging was performed
863 with SDCM (sCMOS Orca Flash4 v2 camera) on a single plane. Triple-positive vesicles are
864 highlighted with a purple circle tracking the spots in the antigen channel. Movie was recorded 10 min
865 after activation and imaged every 2 s.
866
867 **Supplementary Movie 2. Antigen colocalises with acidic vesicles soon after internalisation.** A20
868 D1.3 cells were loaded with LysoTracker (middle panel) and activated with AF488-αIgM (left panel).
869 Right panel shows merge image of antigen channel (magenta) and LysoTracker channel (cyan). Live-
870 imaging was performed with SDCM (EVOLVE camera) on a single plane every 500 ms. Doble-
871 positive vesicles are highlighted with a purple circle tracking the spots in the antigen channel. Movie
872 was recorded 1 min after activation.
873
874 **Supplementary Movie 3. Antigen vesicles fuse with LysoTracker-positive vesicles hovering**
875 **beneath the plasma membrane.** A20 D1.3 cells were loaded with LysoTracker (middle panel) and
876 activated with AF488-αIgM (left panel). Right panel shows merge image of antigen channel
877 (magenta) and LysoTracker channel (cyan). Live-imaging was performed with SDCM (EVOLVE
878 camera) on a single plane every 500 ms. An antigen vesicle fusing with LysoTracker after pinching
879 from the plasma membrane is highlighted with a purple circle. Movie was recorded 80 s after
880 activation.
881
882 **Supplementary Movie 4. Surface MHCII is internalised together with the antigen after**
883 **activation.** A20 D1.3 cells were labelled on ice with AF488-anti-MHCII (left panel) and RRx-αIgM
884 (middle panel). Cells were shifted at 37 ºC to start activation and recorded after 40 s. Right panel
885 shows merge image of antigen channel (magenta) and MHCII channel (cyan). Live-imaging was
886 performed with SDCM (sCMOS Orca Flash4 v2 camera) on a single plane every 4 s. Vesicles positive
887 for MHCII and antigen were tracked with circles (shown in different colours) in the antigen channel.